Improvement of the Elevated Temperature Cycling of $LiMn_2O_4$ spinel for Li Ion Batteries

Seung Hee Woo

Interdisciplinary School of Green Energy

Graduated School of UNIST

2013

Improvement of the Elevated Temperature Cycling of $LiMn_2O_4$ spinel for Li Ion Batteries

Seung Hee Woo

Interdisciplinary School of Green Energy

Graduated School of UNIST

Improvement of the Elevated Temperature Cycling of $LiMn_2O_4$ spinel for Li Ion Batteries

A thesis

Submitted to the Graduate School of UNIST

in partial fulfillment of the

requirements for the degree of

Master of Science

Seung Hee Woo

02. 20. 1013

Approved by

Major Advisor

Kyu Tae Lee

Improvement of the Elevated Temperature Cycling of $LiMn_2O_4$ spinel for Li Ion Batteries

Seung Hee Woo

This certifies that the thesis of Seung Hee Woo is approved.

02. 20. 2013

signature

Thesis supervisor: Kyu Tae Lee

signature

Soojin Park

signature

Nam-Soon Choi

Abstract

Lithium manganese oxide spinel materials have been extensively studied as a cathode material for lithium ion batteries because it is inexpensive, safe, and eco-friendly. One critical shortcoming for this material is, however, the poor cycle stability that is mainly associated with manganese dissolution during extended cycling, especially at elevated temperature (> 50 ^{o}C). To relieve the capacity fading of $LiMn_2O_4$/graphite cells caused by manganese dissolution, we develop the functional binder and separator having ion exchangeability between dissolved Mn ions and Na ions of functional materials. First of all, three ion-exchangeable binders including carboxymethyl cellulose sodium salt (CMC), poly(sodium 4-styrenesulfonate) (PSS), and alginic acid sodium salt (AGA) are compared with the conventional binder of polyvinylidene fluoride (PVdF). From the galvanostatic experiments of $LiMn_2O_4$/graphite full cells at high temperature (60 ^{o}C), the ion-exchangeable binders for graphite anode show a noticeable improvement in the capacity retention. This is attributed to that the dissolved Mn ions are trapped in the ion exchangeable binders due to ion exchange between manganese ions in electrolytes and sodium ions of binders. In other words, the ion-exchangeable binders prevent the reduction of dissolved Mn ions at the surface of graphite anode, resulting in the improvement of cycle performance. This is supported by the analysis using inductively coupled plasma mass spectrometry (ICP-MS) for Mn-dissolved electrolytes and X-ray diffraction (XRD) for lithiated graphite anode. Also, the effect of ion exchange is further examined using an ion exchangeable separator. The surface-modified separator shows the improved cycle retention of $LiMn_2O_4$/graphite full cell at 60 ^{o}C due to ion exchange between manganese ions in electrolytes and sodium ions of separators.

Contents

1. Introduction ……………………………………………………………………………….1

1.1. Lithium-ion batteries ………………………………………………………………….1

1.2. Spinel lithium manganese oxide ………………………………………………….....4

2. Theoretical development ……………………………………………………………...11

2.1. Ion exchange …………………………………………………………………………...11

2.2. Ion exchangeable binder and separator …………………………………………...12

3. Experimental ……………………………………………………………………………13

3.1. Ion-exchangeable binder ……………………………………………………………13

3.1.1. Electrochemical measurements …………………………………………………13

3.1.2. Supporting Experimental …………………………………………………………13

3.2. Ion-exchangeable separator …………………………………………………………14

3.2.1. Modification of separator ………………………………………………...…14

3.2.2. Electrochemical measurements ……………………………………………...…14

3.2.3. Supporting Experimental ……………………………………………….………14

3.3. Characterization ………………………………………………………….…………15

4. Results and discussion ……………………………………………………...…………18

5. Conclusion …………………………………………………………………………….39

6. References …………………………………………………………...……………..40

List of figures

Figure 1. Comparison of the different battery technologies in terms of volumetric and gravimetric energy density.

Figure 2. Schematic illustration of the first Li-ion battery ($LiCoO_2/Li^+$ electrolyte/graphite).

Figure 3. Structure of $LiMn_2O_4$ spinel.

Figure 4. a) Initial charge and discharge curves of $Li_{1.04}Mn_{1.98}O_4$ cathode, lithium metal anode, and 1 M $LiPF_6$ in EC:DMC (1:2) at a current density of 0.5 mA/cm^2 at 25 ^oC, and b) Cycle performance.

Figure 5. Schematic illustrations of a spinel skeleton structure. a) top view and b) side view of 'spinel' structure. Large and small regular squares in a) indicate cubic and tetragonal unit cells, respectively.

Figure 6. Schematic illustration for the manganese dissolution out of a delithiated lithium manganese oxide cathode (a) by HF attack and (b) by anion oxidation.

Figure 7. Discharge capacity for spinel $LiMn_2O_4$ and doped $LiMn_{2-x}Ni_xO_4$ (x=0.01, 0.02, 0.04, and 0.06).

Figure 8. a) A schematic diagram of the coating procedure and b) discharge capacity of the uncoated spinel nanorods, bulk spinel particles, and coated spinel nanoparticles at 65 ^oC in coin-type half cells.

Figure 9. a) Discharge profiles of $Li_{1.1}Mn_{1.9}O_4$/graphite cells charged in EC/EMC/1 M $LiPF_6$ with (a) 5 wt % FEC and (b) 2 wt % VC. The specific capacities obtained were based on the weight of $Li_{1.1}Mn_{1.9}O_4$ in a cell. b) XRD patterns of graphite anodes charged in EC/EMC/1 M $LiPF_6$ with (a) 5 wt % FEC and (b) 2 wt % VC before and after being stored at 60 ^oC.

Figure 10. a) Expanded view of polystyrene bead and b) water softening.

Figure 11. Schematic presentation for functional roles of ion-exchangeable binder.

Figure 12. Schematic presentation for functional roles of ion-exchangeable separator.

Figure 13. Schematic diagram of grafting of terephthalic acid with ALD on separator.

Figure 14. XRD patterns of a) $Li_{1.1}Mn_{1.86}Mg_{0.04}O_4$ and b) natural graphite.

Figure 15. SEM images of a-b) $Li_{1.1}Mn_{1.86}Mg_{0.04}O_4$ and c-d) natural graphite.

Figure 16. Electrochemical performances of $Li_{1.1}Mn_{1.86}Mg_{0.04}O_4$ half cell with Li metal: a) cyclability, b) voltage profiles at 30 ^oC, and c) 60 ^oC.

Figure 17. Electrochemical performances of $Li_{1.1}Mn_{1.86}Mg_{0.04}O_4$ (PVdF) / graphite (PVdF) full cell: a) cyclability, b) voltage profiles at 30 ^oC, and c) 60 ^oC.

Figure 18. Structures of a) polyvinylidene fluoride (PVdF), b) carboxymethyl cellulose sodium salt (CMC), c) poly(sodium 4-styrenesulfonate) (PSS), and d) alginic acid sodium salt (AGA).

Figure 19. First and second cycles of graphite with a) PVdF, b) CMC, c) PSS, and d) AGA as binder.

Figure 20. Electrochemical performances of $Li_{1.1}Mn_{1.86}Mg_{0.04}O_4$ (PVdF) / graphite (binder) full cell at 30 ^oC: a) cyclability, b) capacity retention, voltage profiles $Li_{1.1}Mn_{1.86}Mg_{0.04}O_4$ (PVdF) full cell with c) graphite (PVdF), d) graphite (CMC), e) graphite (PSS), and f) graphite (AGA).

Figure 21. Electrochemical performances of $Li_{1.1}Mn_{1.86}Mg_{0.04}O_4$ (PVdF) / graphite (binder) full cell at 60 ^oC: a) cyclability, b) capacity retention, voltage profiles $Li_{1.1}Mn_{1.86}Mg_{0.04}O_4$ (PVdF) full cell with c) graphite (PVdF), d) graphite (CMC), e) graphite (PSS), and f) graphite (AGA).

Figure 22. Mn and Na concentrations in an electrolyte before and after storage with binders.

Figure 23. FT-IR spectra for alginic acid sodium salt before and after storage in the manganese-dissolved solution.

Figure 24. XRD patterns of lithiated graphite prepared with a) PVdF and b) CMC binder.

Figure 25. SEM images of a) PE bare separator and b) PE separator after 10 cycles ALD.

Figure 26. FT-IR spectra of separator according to priority of reaction.

Figure 27. XPS profile of separator synthesized with terephthalic acid grafted with iodine.

Figure 28. Electrochemical performances of $Li_{1.1}Mn_{1.86}Mg_{0.04}O_4$ (PVdF) / graphite (binder) full cell at 60 ^oC: a) cyclability, b) capacity retention, and c) voltage profiles of full cell with ion-exchangeable separator.

List of tables

Table 1. Electrochemical measurement condition.

1. Introduction

1.1. Lithium-ion batteries

The rapid development of innovative technologies raised the need for new and efficient power source systems. In response to the need, advanced and environmental friendly batteries has been developed to replace the nickel-cadmium (Ni-Cd) or nickel-hydride (Ni-MH) batteries. The motivation for using a battery technology based on lithium metal as anode relied initially on the fact that lithium is the most electropositive (-3.04 V versus standard hydrogen electrode) as well as the lightest (equivalent weight M = 6.94 g mol^{-1}, and specific gravity ρ = 0.53 g cm^{-3}) metal, thus facilitating the design of storage systems with high energy density. The advantage in using lithium metal was first demonstrated in the 1970s with the assembly of primary lithium cells. A strong research effort then was mounted to convert lithium primary cells into rechargeable cells with high energy density. In 1972, Exxon used TiS_2 as the positive electrode, lithium metal as the negative electrode and lithium perchlorate in dioxolane as the electrolyte. The early rechargeable lithium cells were plagued with safety problems caused by the tendency of lithium metal anodes to form dendrites and powder deposits on recharging. To circumvent the safety issues surrounding the use of lithium metal, several alternative approaches were pursued in which either the electrolyte or the negative electrode was modified. The first approach involved substituting metallic lithium for a lithium intercalation material as an anode. The concept was first demonstrated in the laboratory by Murphy *et al.* and then by Scrosati *et al.* and led, at the end of the 1980s and early 1990s, to the so-called Li-ion technology and the C/$LiCoO_2$ lithium-ion cell first commercialized by Sony Co. in 1991.[1-3]

Many of the lithium battery cathode materials have a layered structure, which enables the two-dimensional diffusion of the lithium-ion. Layered lithium transition metal oxides arguably represent the most successful category of positive electrode, comprising compounds with formula of $LiMO_2$ (M: Mn, Co, and Ni) that crystallize in a layered structure. The main cathode material, $LiCoO_2$, is widely used in commercial Li ion batteries, de/intercalating Li around 4 V, and has been improved in terms of rate capability and capacity. Although the reversible delithiation of $LiCoO_2$ beyond 0.5 Li is feasible, alternatives to $LiCoO_2$ are necessary because of its high cost, toxicity, and poor safety that make it unsuitable for electric vehicles (EVs) and large-scale energy-storage applications. Initially, the use of layered $LiNiO_2$ was considered, as this displayed favourable specific capacity of 200 mA h g^{-1} compared to only 140 mA h g^{-1} for $LiCoO_2$. But expectations were dismissed for safety reasons after exothermic oxidation of the organic electrolyte with the collapsing delithiated Li_xNiO_2 structure. Delithiated Li_xCoO_2 was found to be more thermally stable that its Li_xNiO_2 counterpart. Thus, substitution of Co for Ni in $LiNi_{1-x}Co_xO_2$ was adopted to provide a partial solution to the safety concerns surrounding $LiNiO_2$.

Another line of investigation involved the synthesis by soft chemistry of the layered $LiFeO_2$ and $LiMnO_2$ phase to take advantage of the Fe^{4+}/Fe^{3+} or Mn^{4+}/Mn^{3+} redox couples, respectively. In spite of the numerous and diverse synthesis methods attempts to prepare electrochemically attractive $LiFeO_2$ phases failed. In contrast, research on $LiMnO_2$ has been more fruitful, and the structural instability of the layered phase reversing to the spinel $Li_xMn_2O_4$ upon cycling has been diminished through cationic substitution.

Studies to inhibit the transformation led to solid-solution approaches to $LiMO_2$ (M = Ni, Mn, Co, etc/) that could be considered as compensation one metal's disadvantage with another's advantage. Reversible capacities exhibited by $LiNi_{0.5}Mn_{0.5}O_2$ were reported to be 200 mA h g^{-1} (2.5-4.5 V window *vs.* Li/Li^+) with little capacity fading. Other advantages of $LiNi_{0.5}Mn_{0.5}O_2$ are lower thermal runaway, better structural thermal stability than $LiCoO_2$ or $LiNiO_2$, and greater inhibition to reaction with electrolytes in the charges state. The metals Co, Ni, and Mn can all be accommodated in the layered metal oxide structure, to give a range of composition $Li[Co_xNi_yMn_z]O_2$ ($x + y + z = 1$). One composition, $LiCo_{1/3}Ni_{1/3}Mn_{1/3}O_2$ reported in 2001 by Ohzuku et al., has shown particularly promising electrochemistry and intriguing structural behavior. The material shows good rate capability (200 mA h g^{-1} at 18.3 mA g^{-1} and 150 mA h g^{-1} at 1600 mA g^{-1}). Another attractive property is its excellent safety properties at a high state of charge, compared to $LiNiO_2$ and $LiCoO_2$.

In the search for improved materials for positive electrodes, it has been recognized recently that olivine (magnesium iron silicate) oxyanion scaffolded structures, built from corner-sharing MO_6 octahedra (where M is Fe, Ti, V or Nb) and XO_4^{n-} tetrahedral anions (where X is S, P, As, Mo or W), offers interesting possibilities. Polyoxyanionic structures possess M-O-X bonds; altering the nature of X will change (through an inductive effect) the iono- covalent character of the M-O bonding. In this way it is possible to systematically map and tune transition-metal redox potentials. For instance, with the use of the phosphate polyanions PO_4^{3-}, the Fe^{3+}/Fe^{2+} and V^{4+}/V^{3+} redox couples lie at higher potentials than in the oxide form. One of the main drawbacks with using these materials is their poor electronic conductivity, and this limitation had to be overcome through various materials processing approaches, including the use of carbon coatings, mechanical grinding or mixing, and low-temperature synthesis routes to obtain tailored particles. $LiFePO_4$, for example, can presently be used at 90% of its theoretical capacity (165 mA h g^{-1}) with decent rate capabilities, and thus is a serious candidate for the next generation of Li-ion cells.[3-7]

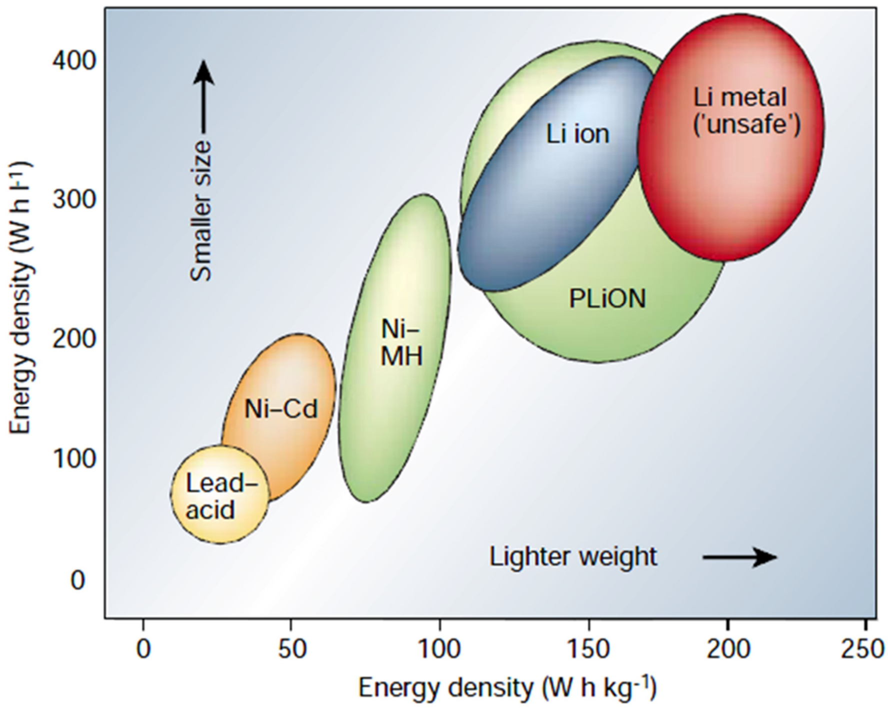

Figure 1. Comparison of the different battery technologies in terms of volumetric and gravimetric energy density.

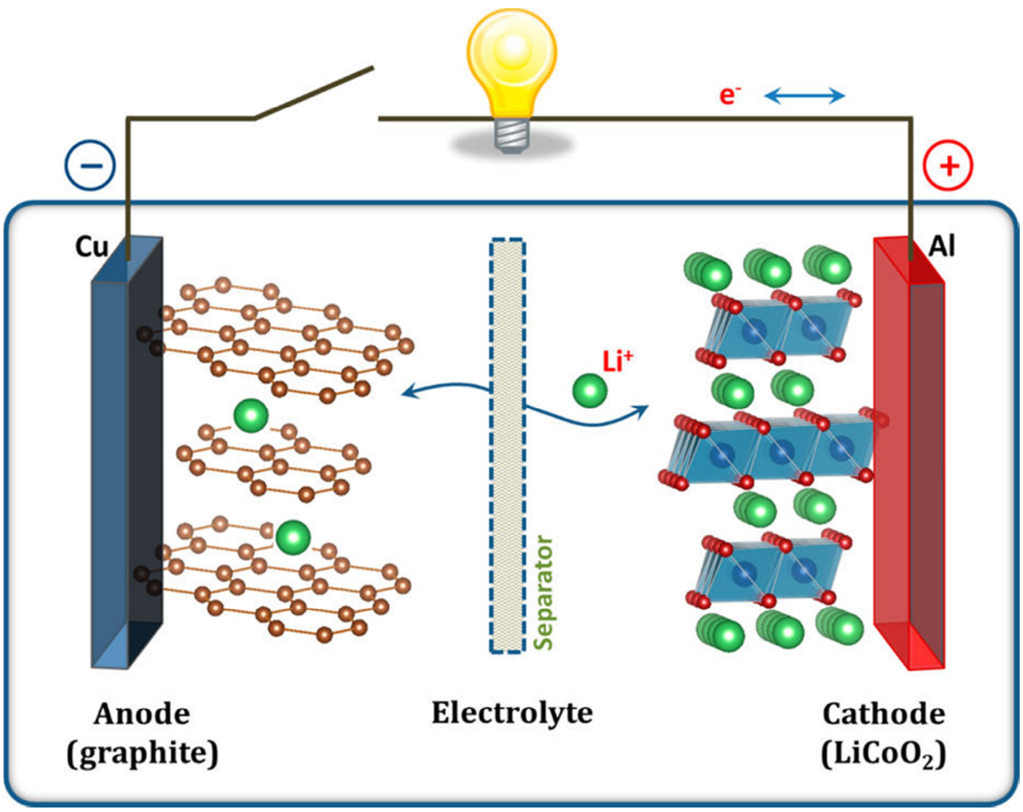

Figure 2. Schematic illustration of the first Li-ion battery ($LiCoO_2/Li^+$ electrolyte/graphite).

1.2. Spinel lithium manganese oxide

Manganese, whose resource is abundant and inexpensive, is used worldwide as an environmentally friendly and inexpensive dry battery material. Moreover, when a spinel type manganese-based material is used as the electrode material of a lithium-ion battery, the battery has the advantages of greatly improved safety and an inexpensive battery control circuit. The market trend for the manganese-based cathode material in a lithium-ion battery is roughly divided into two categories. The first category is materials used in portable electronic devices such as the mobile phone. And the second category is the cathode materials for large size lithium-ion batteries as power sourced for electric vehicles, hybrid vehicles, and so forth. High power, safety, and low cost are strongly required among their performances, so manganese-based cathode materials are suitable for such applications. It overwhelmingly excels in the power density compared to cheaper iron-based cathode material ($LiFePO_4$) and it is used in a large-sized battery. The spinel type manganese oxide has been used for the main cathode material of the lithium-ion battery as a power source for the hybrid vehicle and the electric motorcycle. Although the iron-based material ($LiFePO_4$), which is expected to succeed the manganese-based cathode material, is being studied all over the world; it has not reached practical use yet because of its poor electric conductivity and its complicated synthesis method.[3, 8-12]

At ambient temperature, the crystal structure of $LiMn_2O_4$ belongs to the Fd3m space group of a cubic system; lithium ions occupy the tetrahedral 8a site, manganese ions the octahedral 16d site and oxygen ions the 32e site (Fig. 3). Since the average valence of manganese ions in $LiMn_2O_4$ is 3.5, the same amounts of Mn^{3+} and Mn^{4+} ions are distributed randomly on the 16d site. That is, the distribution of cations in $LiMn_2O_4$ can be represented by the following ionic formula: $(Li^+)_{8a}[Mn^{3+}Mn^{4+}]_{16d}O^{-2}_4$. According to neutron and x-ray diffraction analyses, the Mn_2O_4 spinel framework remains during the insertion of excess lithium into $LiMn_2O_4$ as well as during lithium extraction from the stoichiometric material. In other words, the process of the insertion and the extraction of Li^+ is found to be via intercalation of Li^+ between two layers consisting of MnO_6 octahedra.[9-12]

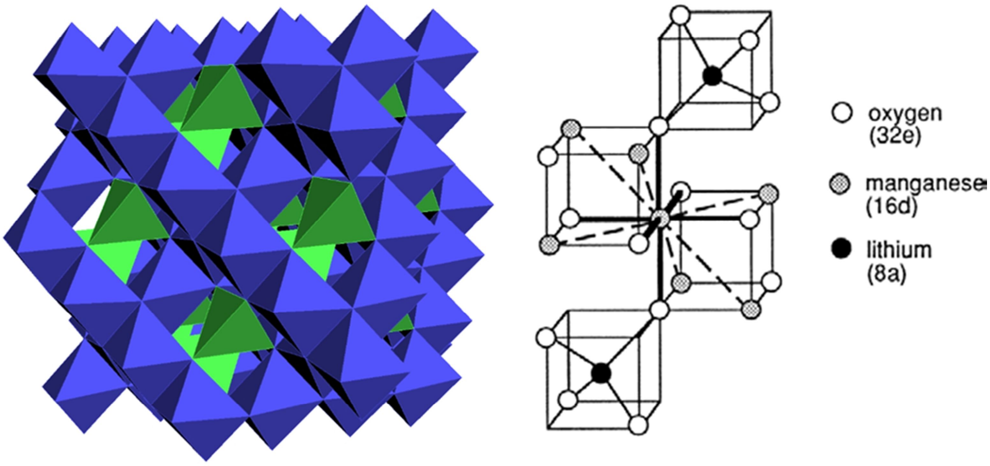

Figure 3. Structure of $LiMn_2O_4$ spinel.

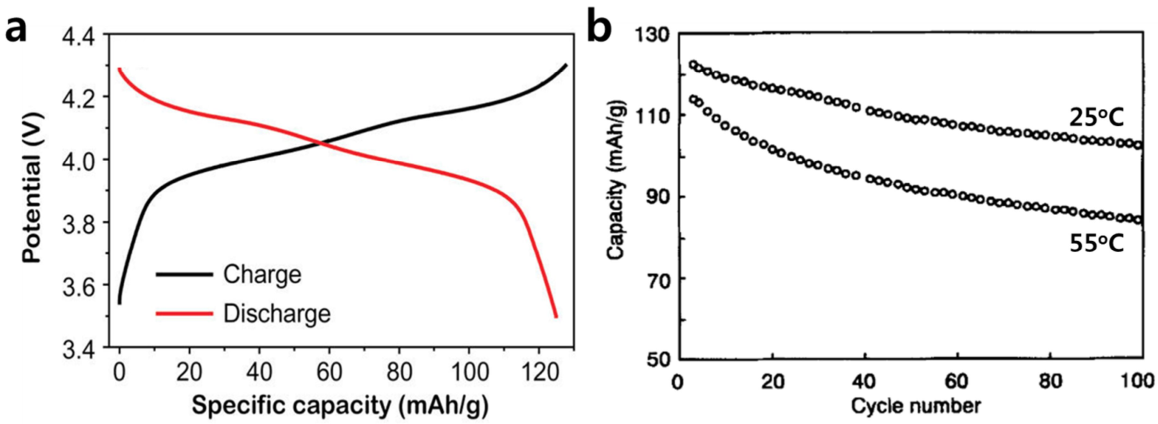

Figure 4. a) Initial charge and discharge curves of $Li_{1.04}Mn_{1.98}O_4$ cathode, lithium metal anode, and 1 M $LiPF_6$ in EC:DMC (1:2) at a current density of 0.5 mA/cm^2 at 25^{o}C, and b) Cycle performance.

The 4-V region of $LiMn_2O_4$ consists of two smooth plateaus (Fig. 4a): the 4.0-V region (low-voltage plateau) and the 4.15-V region (high-voltage plateau). Here, the charge/discharge product of $LiMn_2O_4$ is expressed as $Li_{1-x}Mn_2O_4$. The low-voltage plateau ($x < 0.5$) is a single-phase region where the a-axis of spinel $Li_{1-x}Mn_2O_4$ successively shrinks as the increase in x. The high-voltage plateau ($x >$ 0.5) is a two-phase region where two cubic phases with different lattice parameter, $Li_{0.5}Mn_2O_4$ and λ-MnO_2, coexist. Figure 4b shows the decay of the discharge capacity with cycling. After 100 cycles, the discharge capacities at 25 and 55 °C were 102 and 84 mAh/g, respectively. Their capacity loss is 15% at 25 °C and 28% at 55 °C, respectively. The elevated temperature thus accelerates the capacity fading. Several mechanisms such as Jahn-Teller distortion of Mn^{3+}, Mn dissolution into the electrolyte; loss of crystallinity; development of microstrain due to lattice mismatch between two distinct cubic phases formed on cycling; and an increase in oxygen deficiencies or oxygen loss upon cycling have all been suggested to be the source of capacity fade. [13-19]

Some spinel-structured manganese oxides, such as $MnMn_2O_4$ (hausmannite), $ZnMn_2O_4$ (hetaerolite), etc., show a tetragonal symmetry $I4_1/amd(D_{4h}{}^{19})$ due to Jahn-Teller distortion of a $Mn^{3+}O_6$-octahedron. Although the crystal structures are quite different between the two structures from an x-ray crystallographic point of view, MnO_6-octahedral linkage to form these two structures is exactly the same as was illustrated in Figure 5 Large and small regular squares indicate a cubic unit cell and that of a tetragonal unit cell, respectively. From a relation between cubic and tetragonal setting in a lattice, one can convert a cubic unit cell parameter, a_c, into tetragonal unit cell parameters, a_T and c_T and also Miller indexes (h, k, l) for $I4_1$/amd are converted into (h + k, h - k, l) for Fd3m. Such an anisotropic change in a unit cell dimension is derived from a change in a local symmetry of a MnO_6-octahedron from O_h to approximate D_{4h}, i.e., Jahn-Teller distortion of MnO_6-octahedron. It is worthwhile to note that Jahn-Teller distortion of a MnO_6-octahedron begins at the composition of $Li_{1.0}Mn_2O_4(MnO_{1.75})$ at which half of the octahedral Mn^{4+} ions are already reduced to Mn^{3+} ions in a cubic close-packed oxygen matrix. Consequently, further reduction of this $Li_{1.0}Mn_2O_4$-matrix having a critical composition of being cubic symmetry induce a phase separation to $Li_{1.0}Mn_2O_4$ (cubic) and $Li_{2.0}Mn_2O_4$ (tetragonal). Since the lattice parameters of these two phases are quite different especially in the c_T-axis, a disorder due to an internal stress may exist at an interphase between the cubic and the tetragonal phases. [20-24]

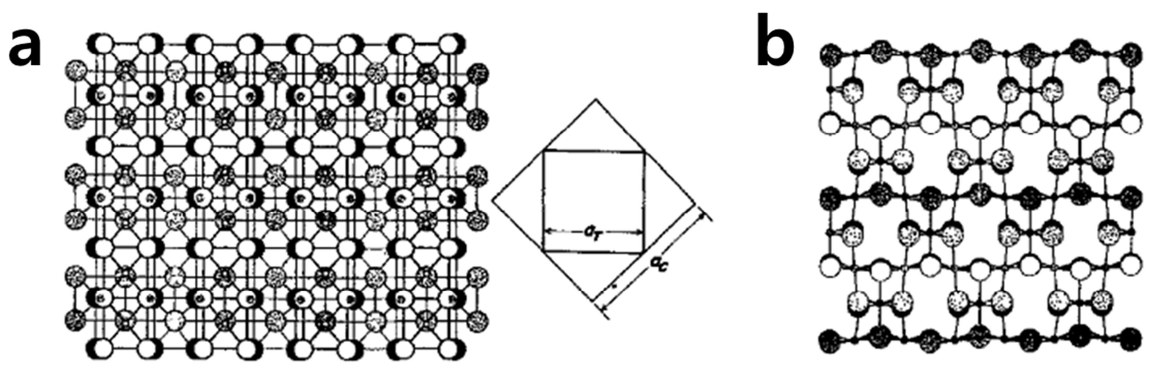

Figure 5. Schematic illustrations of a spinel skeleton structure. a) top view and b) side view of 'spinel' structure. Large and small regular squares in a) indicate cubic and tetragonal unit cells, respectively.

Among various mechanism of capacity fading, Mn dissolution is considered to be the predominant cause (Fig. 6). A considerable dissolution of manganese ions into the electrolyte occurs in the presence of hydrofluoric acid (HF) formed by the hydrolysis of $LiPF_6$ salt. In the discharged state, HF induced manganese dissolution has been found to be the main failure mechanism active at elevated temperatures. It was proposed that $LiPF_6$ salt assists Mn-O bond activation of MnO generated from λ-MnO_2 in the presence of water trace and provokes manganese dissolution.[25-26]

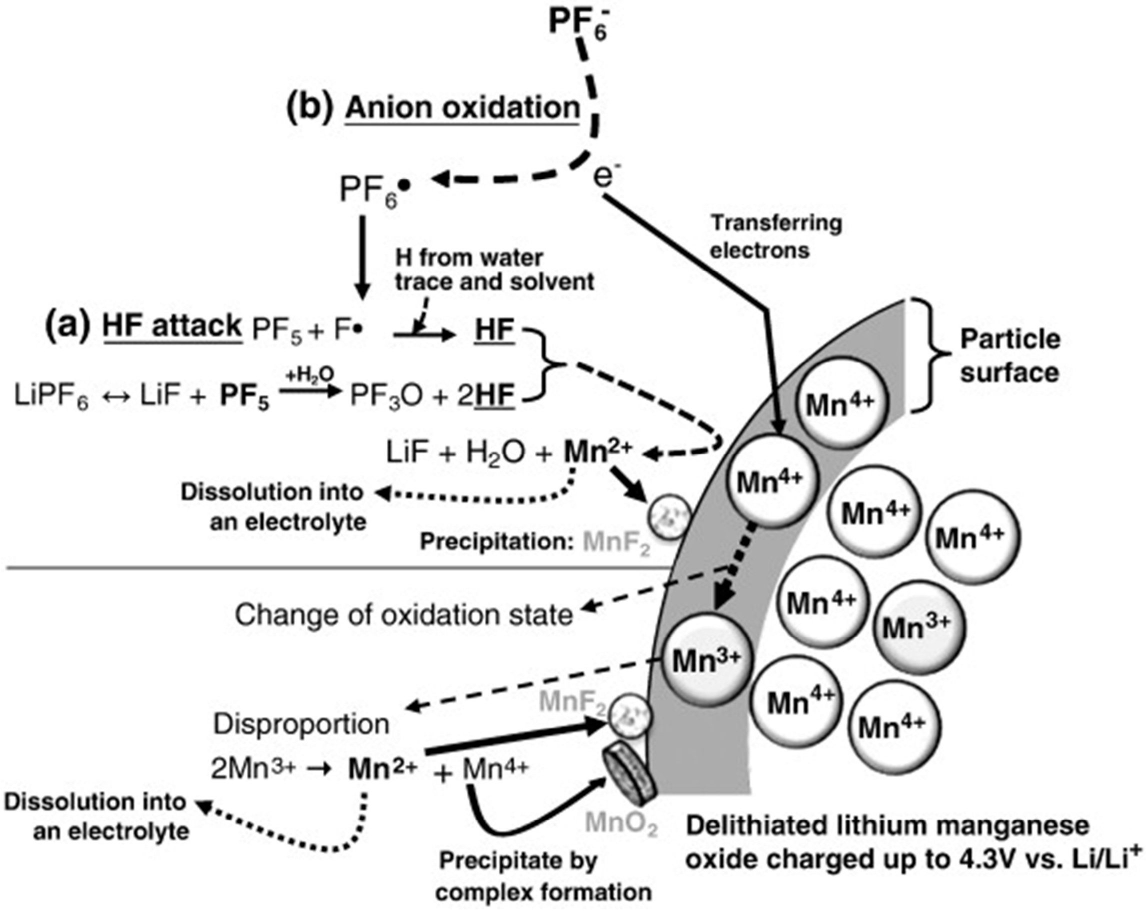

Figure 6. Schematic illustration for the manganese dissolution out of a delithiated lithium manganese oxide cathode (a) by HF attack and (b) by anion oxidation.

To overcome the shortcomings of $LiMn_2O_4$, several approaches have been carried out One way to solve the problem is the substitution of mono-, di-, or trivalent cations in $LiMn_2O_4$ to decrease Mn^{3+} ions which cause disproportion reactions. It was well established that the partial substitution of manganese ions with transition metal ions like Co, Cr, and Ni enhances the structural stability and electrochemical performances of spinel $LiMn_2O_4$. The partial substitution of manganese ions with transition metal ions enhances the structural stability (Fig. 7).[27-37] An alternative approach is to coat the $LiMn_2O_4$ particles with various protective layers of ZrO_2, ZnO, Al_2O_3, and SiO_2. This is because these oxides can suppress Mn dissolution by scavenging HF from the electrolyte (Fig. 8). Protecting the $LiMn_2O_4$ particles from HF in the electrolyte appears successful in improving the structural stability of the cathode and maintaining the capacity of Li-ion batteries. The detailed mechanism of the successful treatments for better performance, however, has not been reported and has yet to be elucidated.[38-43]

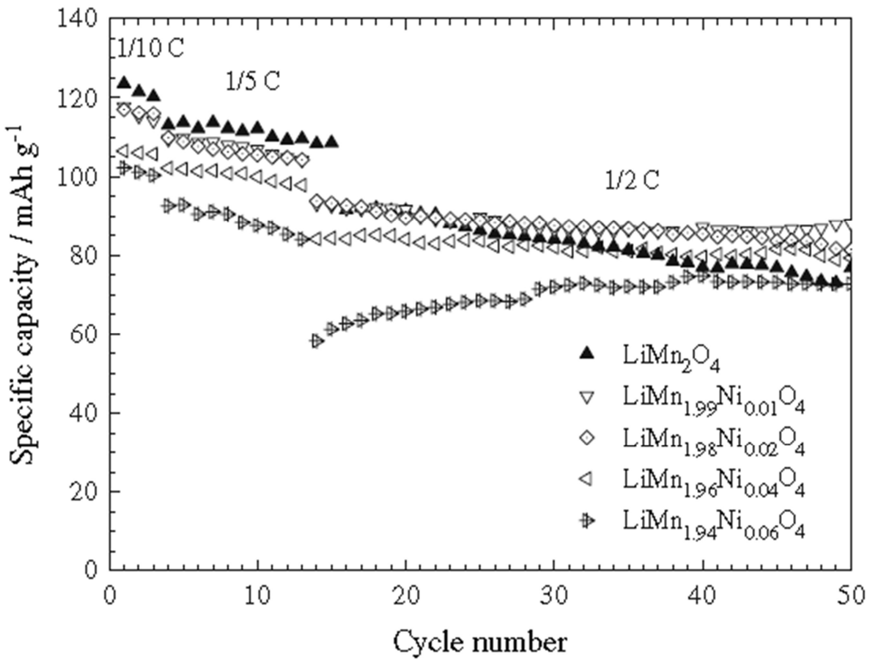

Figure 7. Discharge capacity for spinel $LiMn_2O_4$ and doped $LiMn_{2-x}Ni_xO_4$ (x=0.01, 0.02, 0.04, and 0.06).

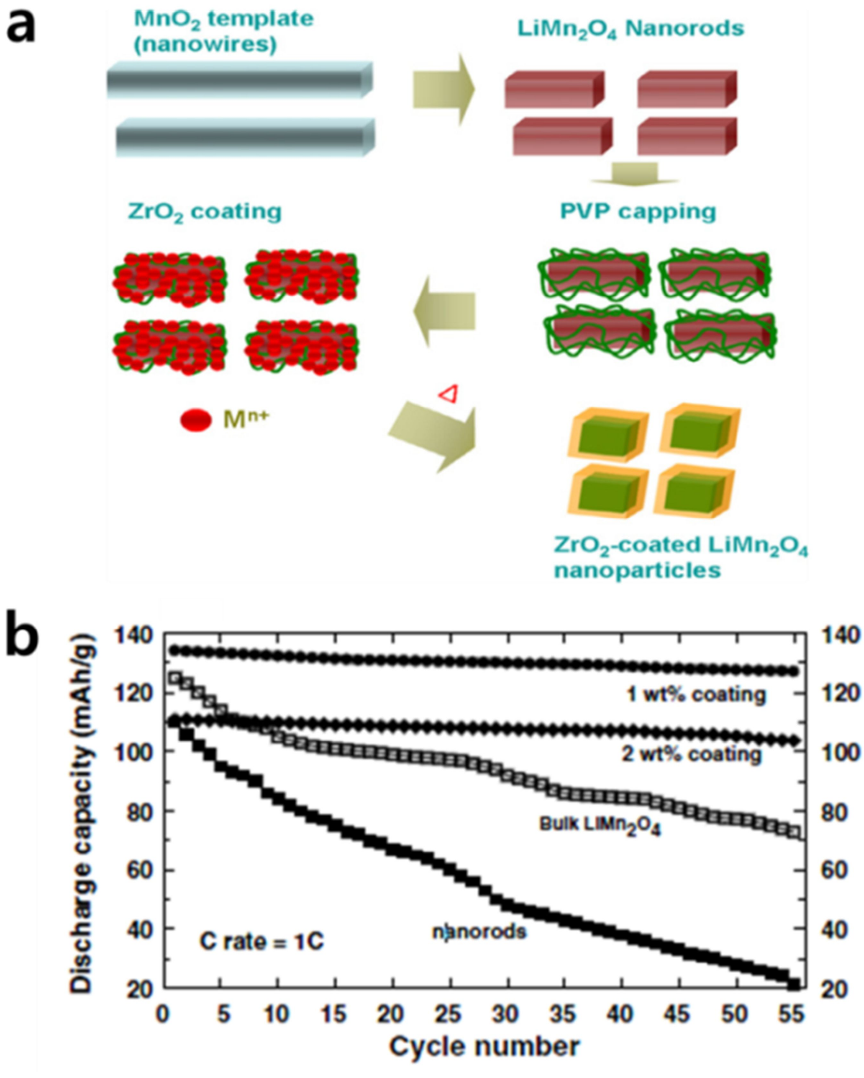

Figure 8. a) A schematic diagram of the coating procedure and b) discharge capacity of the uncoated spinel nanorods, bulk spinel particles, and coated spinel nanoparticles at 65°C in coin-type half cells.

Capacity fading of batteries based on a spinel structure cannot be solely explained by the loss of cathode active materials. Dissolved manganese ions move to the anode and thus lead to the self-discharge of lithiated graphite.[44-45] I. H. Cho et al. applied SEI-forming additive to inhibit Mn deposits on the graphite anode surface and attains a remarkable enhancement of the discharge capacity retention of cells with spinel lithium manganese oxides (Fig. 9).[26]

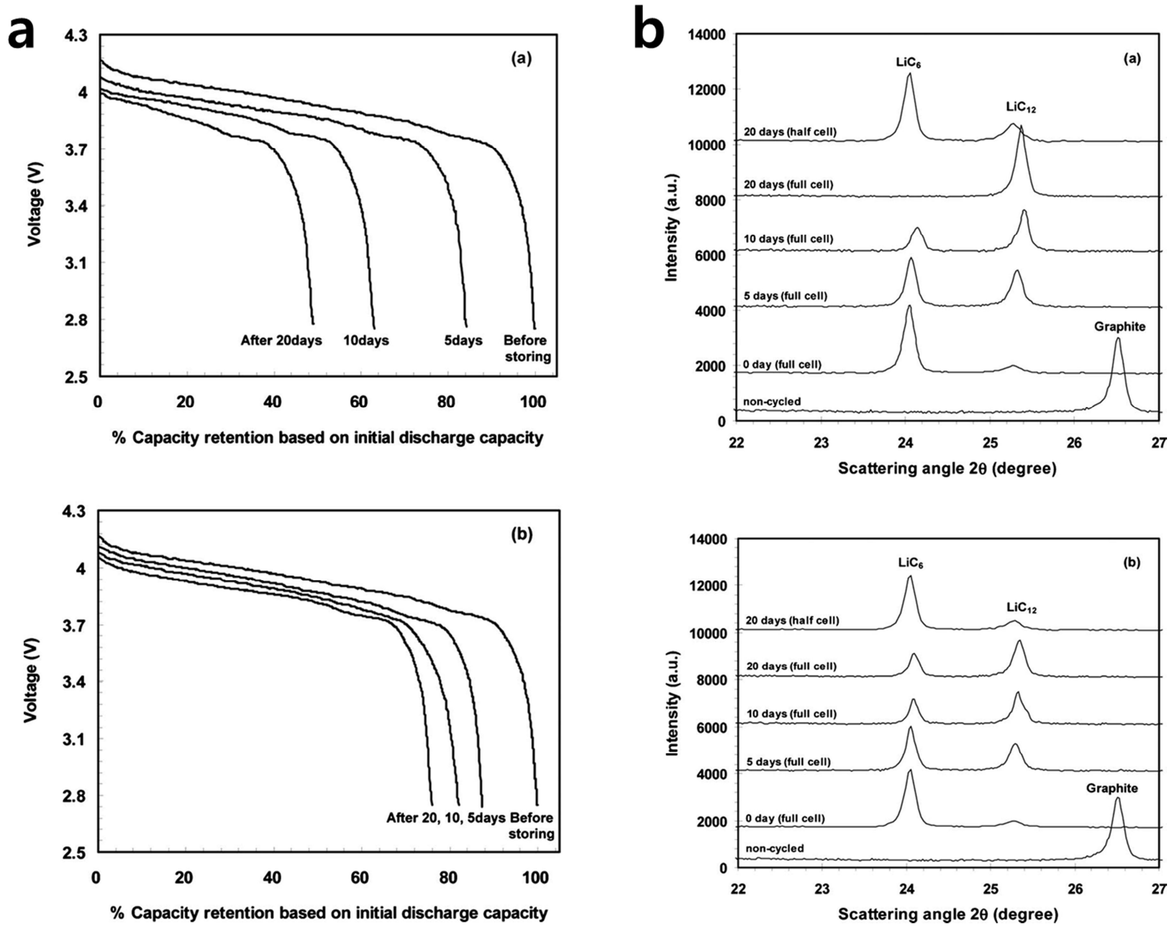

Figure 9. a) Discharge profiles of $Li_{1.1}Mn_{1.9}O_4$/graphite cells charged in EC/EMC/1 M $LiPF_6$ with (a) 5 wt % FEC and (b) 2 wt % VC. The specific capacities obtained were based on the weight of $Li_{1.1}Mn_{1.9}O_4$ in a cell. b) XRD patterns of graphite anodes charged in EC/EMC/1 M $LiPF_6$ with (a) 5 wt % FEC and (b) 2 wt % VC before and after being stored at 60 °C.

2. Theoretical development

2.1. Ion exchange

Ion exchange materials are insoluble substances containing loosely held ions which are able to be exchanged with other ions in solutions which come in contact with them. These exchanges take place without any physical alteration to the ion exchange material. Ion exchangers are insoluble acids or bases which have salts which are also insoluble, and this enables them to exchange either positively charged ions (cation exchangers) or negatively charged ones (anion exchangers). Many natural substances such as proteins, cellulose, living cells and soil particles exhibit ion exchange properties which play an important role in the way the function in nature. Generally the affinity is greatest for large ions with high valency. For dilute solutions the order of affinity for some common cations is approximately:

$Hg^{2+} < Li^{+} < H^{+} < Na^{+} < K^{+} \approx NH^{4+} < Cd^{2+} < Cs^{+} < Ag^{+} < Mn^{2+} < Mg^{2+} < Zn^{2+} < Cu^{2+} < Ni^{2+} < Co^{2+} < Ca^{2+} < Sr^{2+} < Pb^{2+} < Al^{3+} < Fe^{3+}$

Ion exchange resins are polymers that are capable of exchanging particular ions within the polymer with ions in a solution that is passed through them. In water purification the aim is usually either to soften the water. The water is softened by using a resin containing Na^{+} cations but which binds Ca^{2+} and Mg^{2+} more strongly than Na^{+}. As the water passes through the resin the resin takes up Ca^{2+} and Mg^{2+} and releases Na^{+} making for softer water.[46]

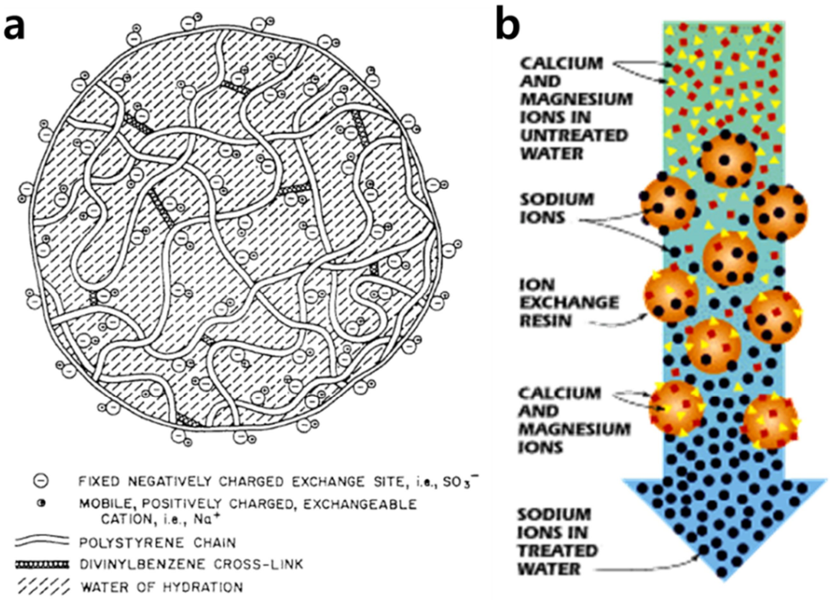

Figure 10. a) Expanded view of polystyrene bead and b) water softening.

2.2. Ion exchangeable binder and separator

We introduce, for the first time, ion-exchangeable binders and separator that have functional groups of sodium carboxylate or sulfonate. These functional groups of binders and separator play a role of ion exchange between Na^+ ions of functional groups and dissolved Mn^{2+} ions of $LiMn_2O_4$ electrodes. This ion exchange traps dissolved Mn^{2+} ions to inhibit the reduction of Mn^{2+} on the surface of lithiated graphite anode, resulting in improved cycle performance at high temperature.

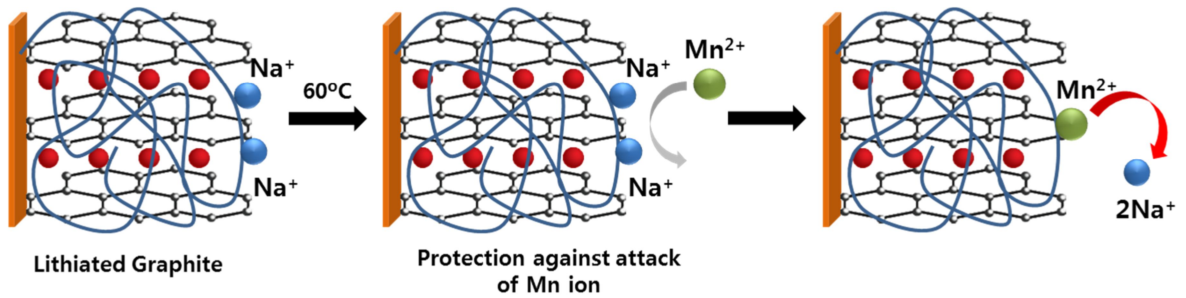

Figure 11. Schematic presentation for functional roles of ion-exchangeable binder.

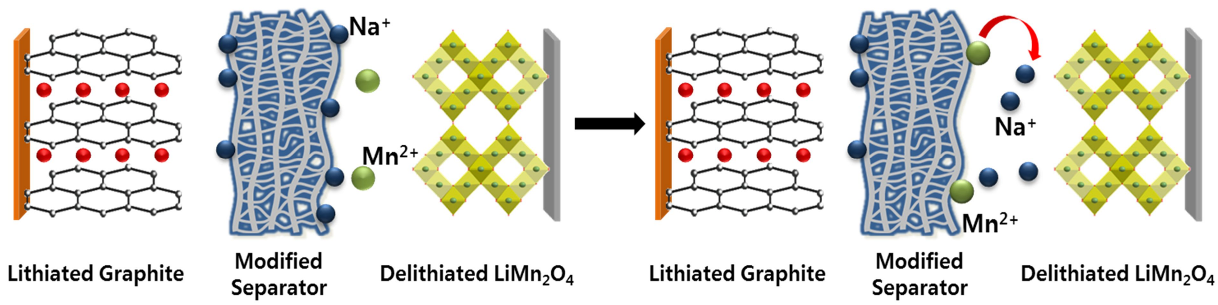

Figure 12. Schematic presentation for functional roles of ion-exchangeable separator.

3. Experimental

3.1. Ion-exchangeable binder

3.1.1. Electrochemical measurements

$Li_{1.1}Mn_{1.86}Mg_{0.04}O_4$ (Mitsui Co., Ltd.) and natural graphite (DAG-87, Sodiff Advanced Material Co., Ltd.) were used as the active materials of the cathode and anode, respectively. Cathodes were prepared by mixing 80 wt.% of $Li_{1.1}Mn_{1.86}Mg_{0.04}O_4$, 10 wt.% of carbon black (Super-P, Timcal Inc.) as a conducting material, and 10 wt.% of polyvinylidene fluoride (PVdF) (KF1000, Kureha Chemical Industry) binder. The slurry was coated onto aluminum foil. Anodes were prepared by mixing 80 wt.% of the natural graphite powder, 10 wt.% of carbon black, and 10 wt.% of binder. Four anode electrodes were made with four binders, PVdF, carboxymethyl cellulose sodium salt (CMC) (Sigma Aldrich), poly(sodium 4-styrenesulfonate) (PSS) (Sigma Aldrich), and alginic acid sodium salt (AGA) (Sigma Aldrich), respectively. The slurries were coated onto copper foil. The electrolyte solution (PANAX E-Tec Co., Ltd.) was composed of a commercially available 1.3 M lithium hexafluorophosphate ($LiPF_6$) dissolved in a solvent mixture of ethylene carbonate (EC) and diethyl carbonate (DEC) with a 3:7 volume ratio.

The coin-type half cells (2016) with $Li_{1.1}Mn_{1.86}Mg_{0.04}O_4$ cathode or nature graphite anode were assembled in an argon filled glove box with a Li metal electrode. For $Li_{1.1}Mn_{1.86}Mg_{0.04}O_4$ cathode galvanostatic experiments were performed at a current density of 14.8 mA g^{-1} (ca. 0.1C) and a temperature of 30 ^oC and 60 ^oC in the voltage range of 4.3 and 3.0 V (*vs*. Li/Li^+). For nature graphite anode galvanostatic experiments were performed at a current density of 19 mA g^{-1} (ca. 0.05C) and a temperature of 30 ^oC in the voltage range of 0 and 3.0 V (*vs*. Li/Li^+). The coin-type full cells (2032) with $Li_{1.1}Mn_{1.86}Mg_{0.04}O_4$ cathode and nature graphite anode were assembled in an argon filled glove box. The full cells were cycled between 4.25 and 2.0 V (*vs*. Li/Li^+) at a constant current of 0.1C (10.3 mA g^{-1}) at 30 ^oC and 60 ^oC.

3.1.2. Supporting experimental

To clarify the ion exchange between manganese ions and sodium ions, inductively coupled plasma (ICP) spectrometry was observed. After $Li_{1.1}Mn_{1.86}Mg_{0.04}O_4$ was stored in electrolyte at 60 ^oC for 1 week, electrolyte was obtained with dissolved manganese ions. Then electrolyte containing dissolved manganese ions was restored with powder of five different binders used for nature graphite anodes at room temperature for 1 week and filtered out powder of binder to measure the amount of manganese ions and sodium ions in the electrolytes by means of ICP. Also to identify crystal structure of lithiated graphite depending on the type of binder, after the coin-type half cells (2016) with PVdF binder and CMC binder respectively were lithiated to a potential 0.005 V and kept at 0.005 V for 10 h, they were carefully opened in an argon filled glove box and the electrodes were rinsed in a dimethyl carbonate (DMC) solvent to remove residual electrolyte. They were then stored respectively in electrolyte containing dissolved manganese ions for 5, 10, 30, and 60 min and analyzed by the X-ray diffraction (XRD).

3.2. Ion-exchangeable separator

3.2.1. Modification of separator

Process to prepare ion-exchangeable separator is presented in Figure 13. Al_2O_3 ALD films were grown directly on a porous PE separator at 100 ^oC using a rotary ALD reactor. The precursors utilized for Al_2O_3 ALD were trimethylaluminum (TMA) and H_2O. The separator was then boiled in 30% hydrogen peroxide for 15 min to clean the surface and introduce –OH groups on the surface, which facilitated subsequent surface modification. Clean and dry separator was incubated in 5% solution of (3-aminopropyl)-triethoxysilane (APTES) (Aldrich) in toluene for 8 h. After the reaction, the separator was washed with toluene and deionized water. In the next step, the separator was incubated for 2 h at room temperature with a solution of toluene containing terephthaloyl chloride and washed with deionized water. The terephthalic acid-grafted separator was wet with ethanol and incubated in 0.3 mM sodium hydroxide solution for 8 h at room temperature.

3.2.2. Electrochemical measurements

A coin-type full cell (2032) of $Li_{1.1}Mn_{1.86}Mg_{0.04}O_4$ cathode and nature graphite anode prepared with PVdF binder was assembled respectively with pristine separator and modified separator in an argon filled glove box. The full cell were cycled between 4.25 and 2.0 V (*vs*. Li/Li^+) at a constant current of 0.1C (10.3 mA g^{-1}) at 60 ^oC.

3.2.3. Supporting experimental

As stated in ion-exchangeable binder experimental the amount of exchanged manganese ions for sodium ions was measured by ICP. Pristine separator and modified separator were stored respectively in electrolyte containing dissolved manganese ions at room temperature for 1 week.

3.3. Characterization

Powder XRD data were collected on a Rigaku D/MAX2500V/PC powder diffractometer using Cu-Kα radiation (λ = 1.5405Å) operated from 2θ = 10 - 80°. SEM samples were examined in a Quanta 200 field-emission SEM (FE-SEM) instrument. The atomic composition of the samples was determined by Varian 720-ES inductively coupled plasma (ICP) spectrometry. IR spectra were recorded on a Nicolet FT-IR 200 from Thermo Scientific. Absorption maxima were recorded in wavenumbers (cm^{-1}). Surface analysis was examined with XPS (Thermo Fisher).

Table 2. Electrochemical measurement condition.

Cell type	Cathode (binder)	Anode (binder)	Separator	Voltage window ($vs.$ Li/Li^+)
Half cell	$LiMn_2O_4$ (PVdF)	Lithium metal	Pristine	4.3 – 3.0 V
	graphite (PVdF) graphite (CMC) graphite (PSS) graphite (AGA)	Lithium metal		0 – 3.0 V
Full cell	$LiMn_2O_4$ (PVdF)	graphite (PVdF) graphite (CMC) graphite (PSS) graphite (AGA)		4.25 – 2.0 V
	$LiMn_2O_4$ (PVdF)	graphite (PVdF)	Modificated	

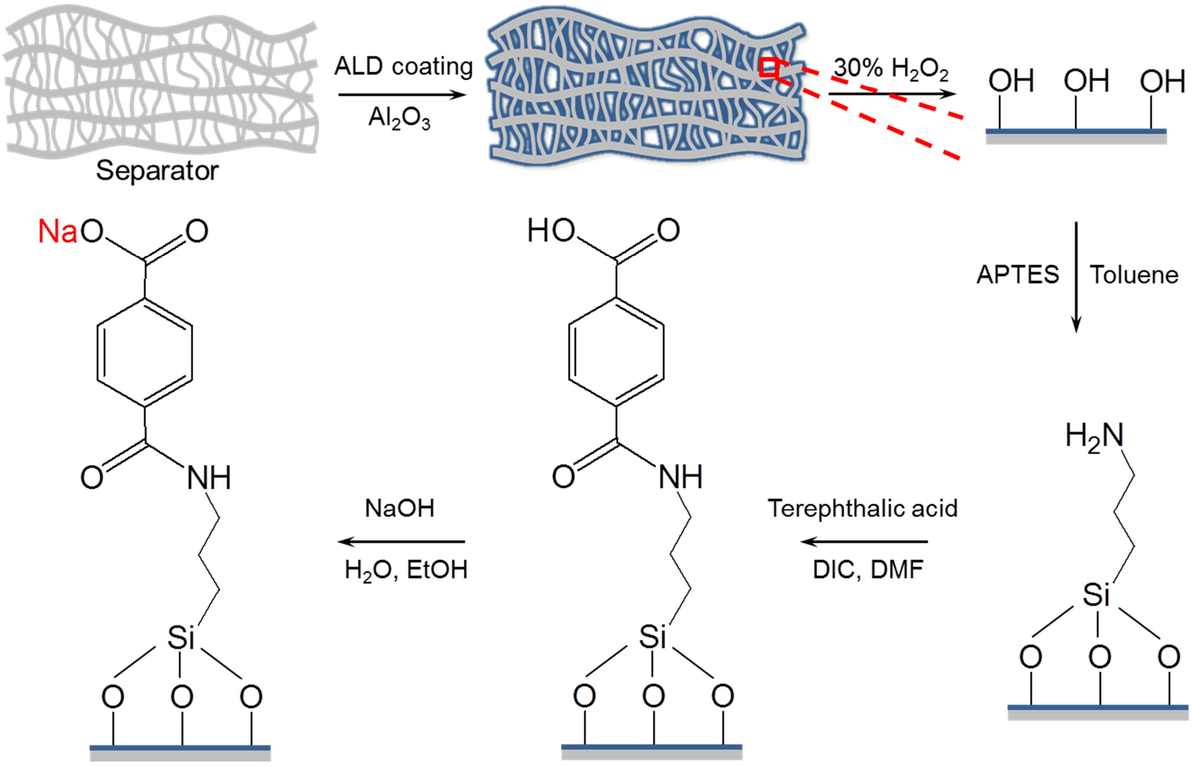

Figure 13. Schematic diagram of grafting of terephthalic acid with ALD on separator.

4. Results and discussion

To emphasize the role of ion exchange on cycle performance at high temperature, the commercialized $Li_{1.1}Mn_{1.86}Mg_{0.04}O_4$ spinel materials (Mitsui Co. Ltd) and DAG-87 nature graphite (Sodiff Advanced Material Co., Ltd.) are used for the evaluation of electrochemical performance. XRD patterns of $Li_{1.1}Mn_{1.96}Mg_{0.04}O_4$ spinel and nature graphite are presented in Figure 14. SEM images are also presented in Figure 15.

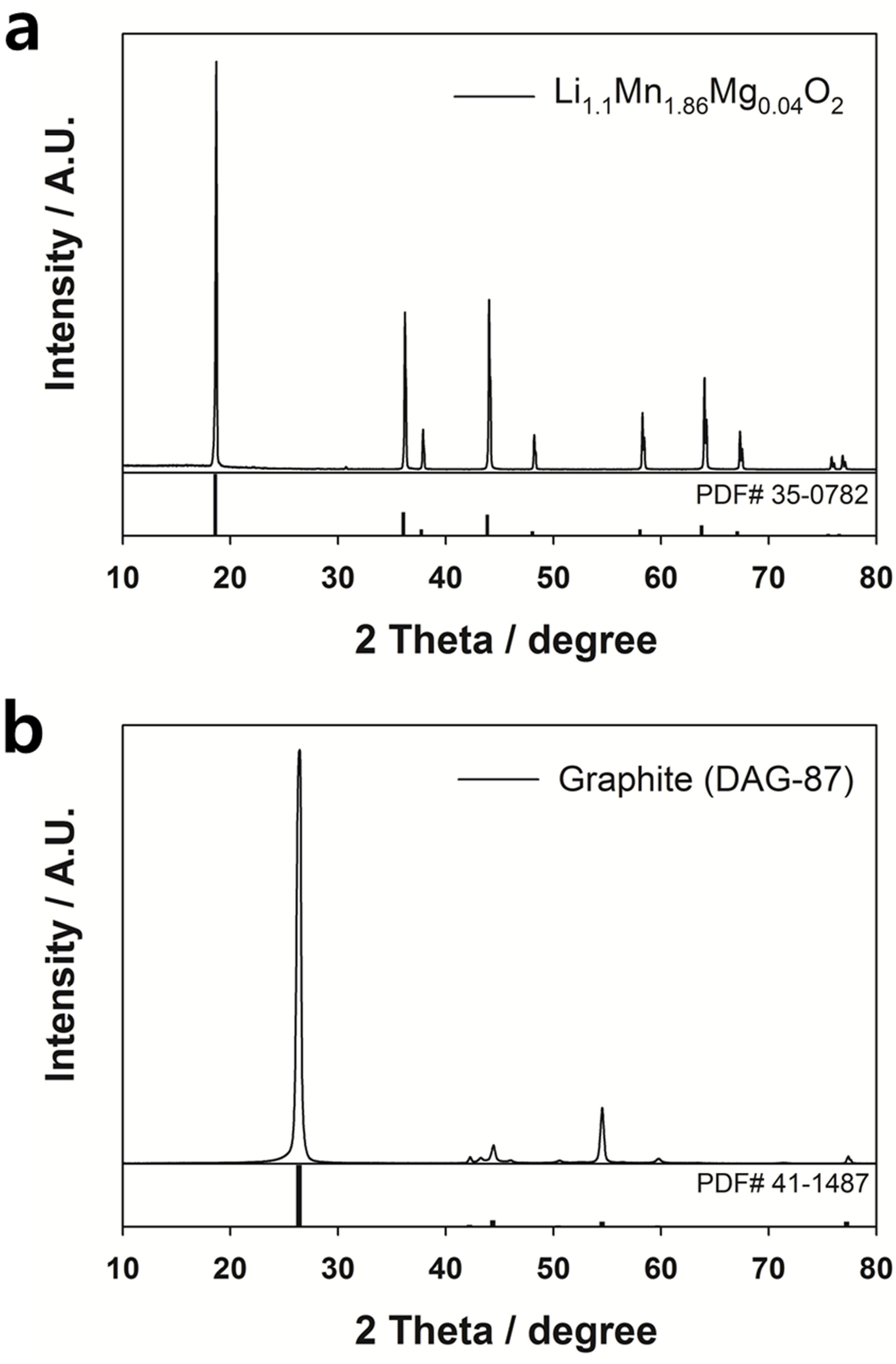

Figure 14. XRD patterns of a) $Li_{1.1}Mn_{1.86}Mg_{0.04}O_4$ and b) natural graphite.

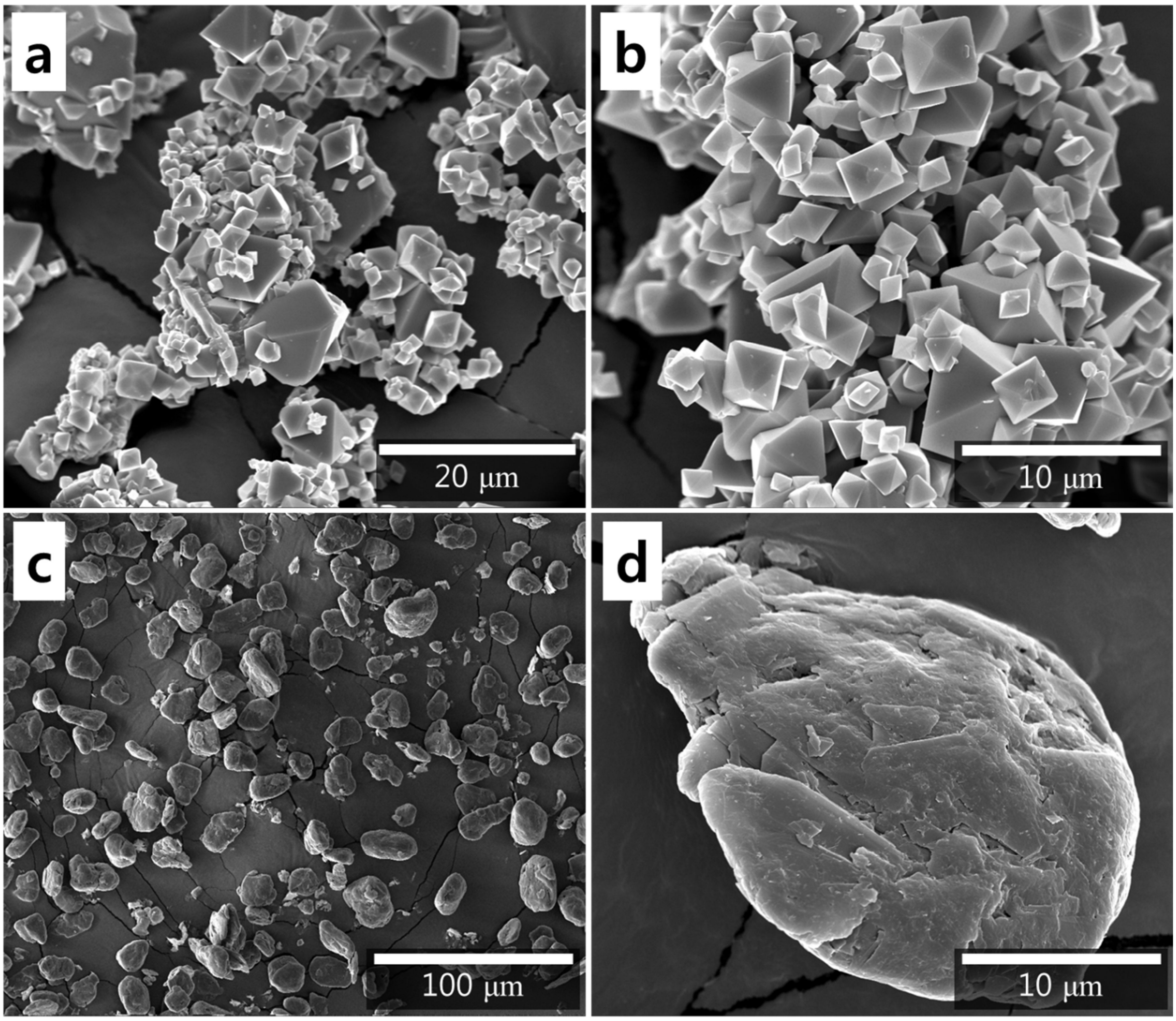

Figure 15. SEM images of a-b) $Li_{1.1}Mn_{1.86}Mg_{0.04}O_4$ and c-d) natural graphite.

$Li_{1.1}Mn_{1.86}Mg_{0.04}O_4$ spinel showed very stable cycle performance at 30 ^oC and even at 60 ^oC, when this is examined using a half cell with Li metal anode (Fig. 16). This electrode exhibited 95% and 90% of capacity retention after 50 cycles at 30 ^oC and 60 ^oC, respectively. This means that the capacity fading of manganese spinels is not mainly caused by the mass loss of active materials, as well known. However, full cells comprised of $Li_{1.1}Mn_{1.86}Mg_{0.04}O_4$ spinel cathode with graphite anode showed different behavior from half cells (Fig. 17). Both electrodes were prepared using a conventional PVdF binder. As shown in Figure 17, full cells showed stable cycle performance at 30 ^oC, but exhibited severe capacity fading at 60 ^oC.

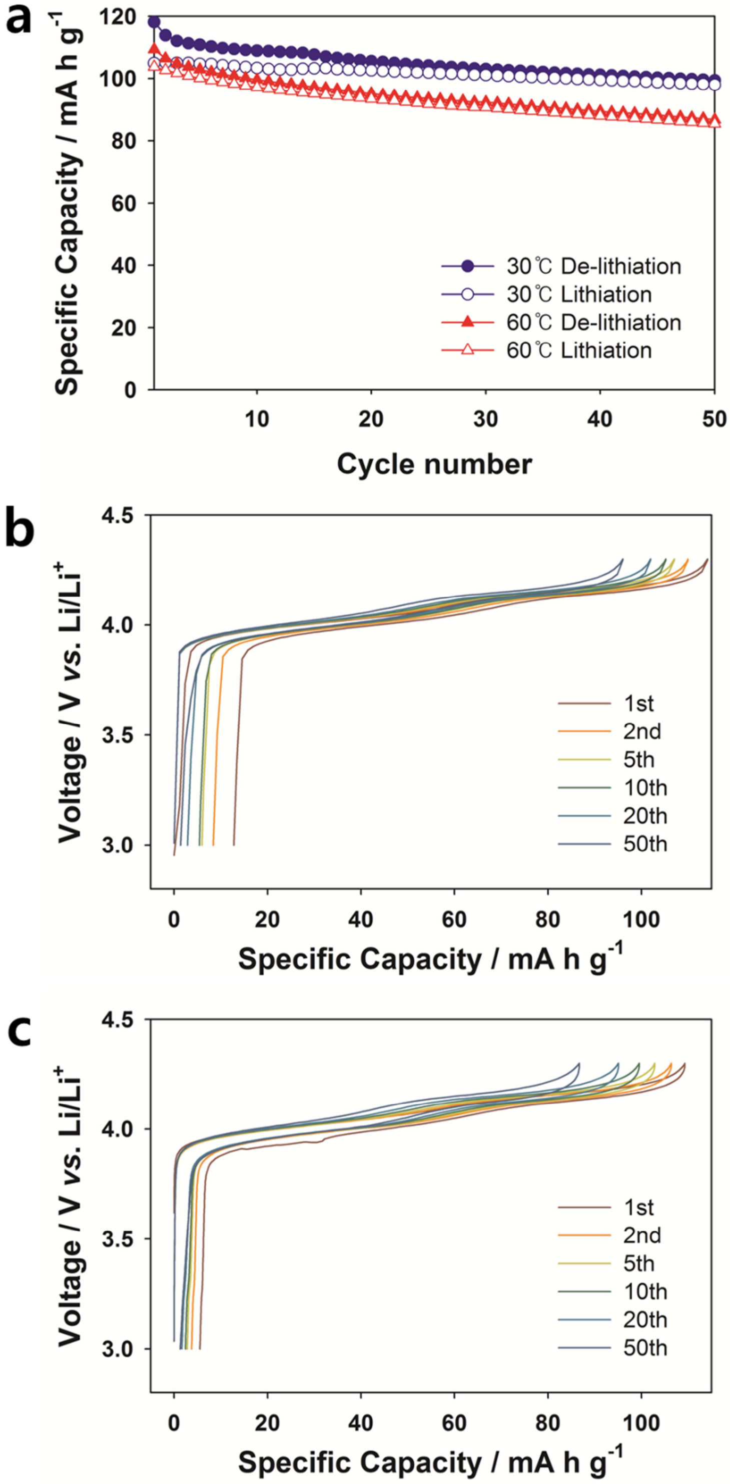

Figure 16. Electrochemical performances of $Li_{1.1}Mn_{1.86}Mg_{0.04}O_4$ half cell with Li metal: a) cyclability, b) voltage profiles at 30 °C, and c) 60 °C.

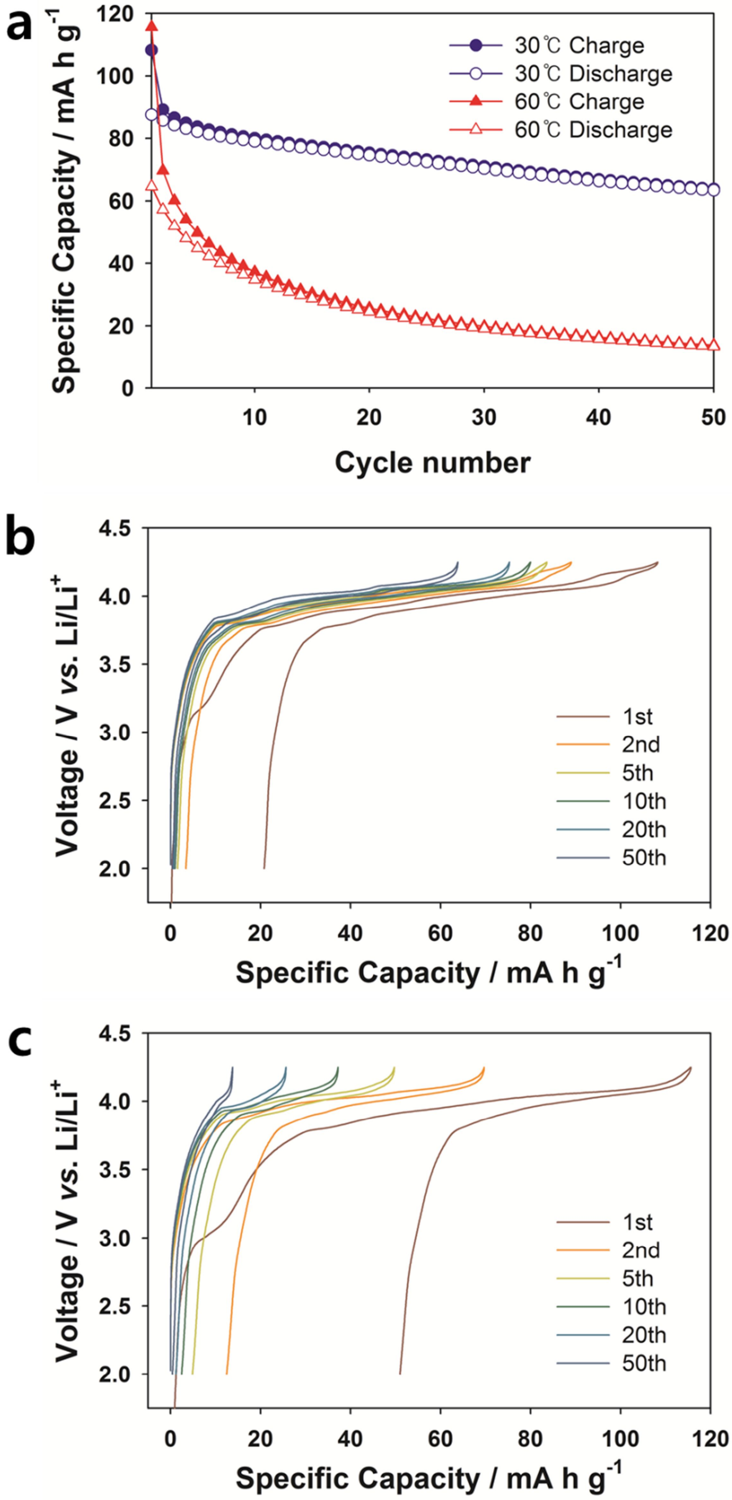

Figure 17. Electrochemical performances of $Li_{1.1}Mn_{1.86}Mg_{0.04}O_4$ (PVdF) / graphite (PVdF) full cell: a) cyclability, b) voltage profiles at 30 ^{o}C, and c) 60 ^{o}C.

As reported previously, this capacity fading at high temperature is attributed to that the dissolved manganese ions cause the self-discharge of lithiated electrodes. Therefore, ion-exchangeable polymers with functional groups of sodium carboxylate and sulfonate including CMC, PSS, and AGA are examined as binders for graphite anodes to alleviate the reduction of dissolved manganese ions on the surface of lithiated graphite anodes (Fig. 18). The concept of ion exchangeable binders is same as the cation exchange resin for water softening. The ion exchange relies on coulombic interaction between the negative charge immobilized on the resin (COO^- or SO^{3-}) and the opposite positive charge of samples (dissolved Mn^{2+} ions). The trapping of Mn^{2+} ions takes place with simultaneous releasing of Na^+ ions from binders due to the stronger coulombic attraction between Mn^{2+} ions and negative charge of binders, as shown in the schematic diagram (Fig. 11), and this process reaches equilibrium with a decreased concentration of manganese ions in electrolytes. Before full cell test, to confirm function of CMC, PSS, and AGA as the binders, half cells of graphite are tested with Li metal (Fig. 19). At first and second cycle voltage profiles of graphite with each binder there is no noticeable difference.

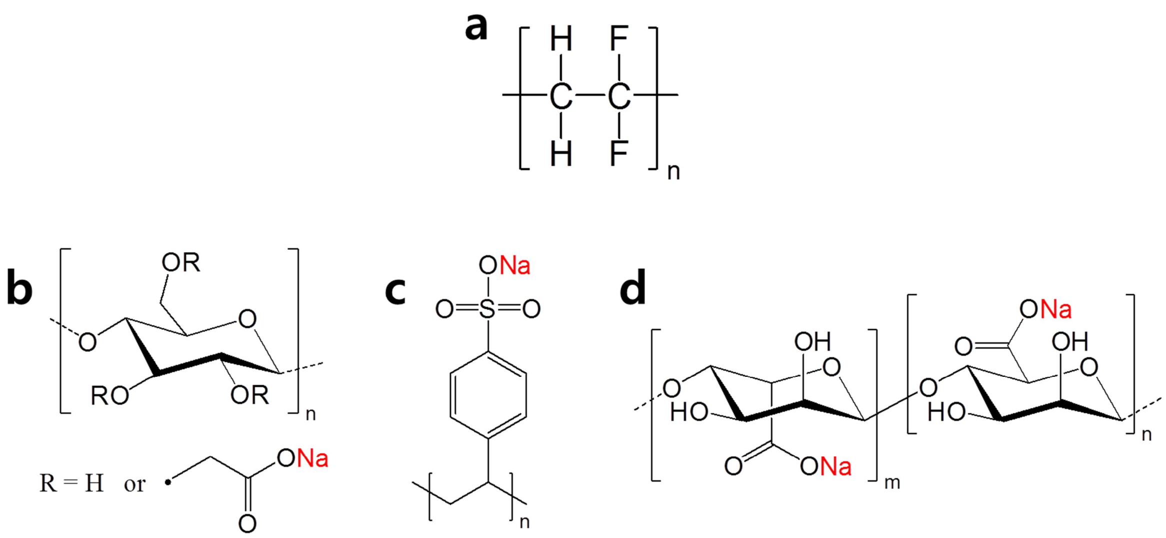

Figure 18. Structures of a) polyvinylidene fluoride (PVdF), b) carboxymethyl cellulose sodium salt (CMC), c) poly(sodium 4-styrenesulfonate) (PSS), and d) alginic acid sodium salt (AGA).

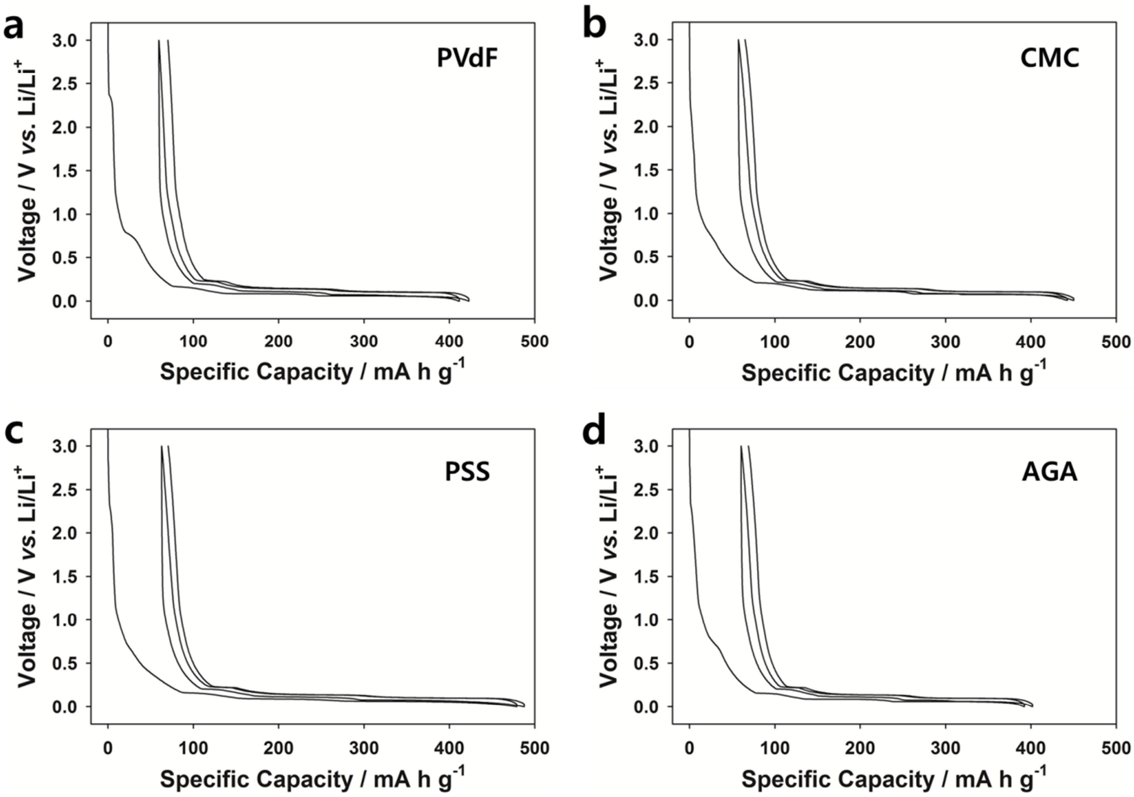

Figure 19. First and second cycles of graphite with a) PVdF, b) CMC, c) PSS, and d) AGA as binder.

Figure 20 shows the cycle performance of full cells at 30 ^oC and the corresponding voltage profiles, respectively. All binders including PVdF and ion exchangeable binders showed similarly stable cycle performance, and this is ascribed by that manganese dissolution is not severe during cycling at 30 ^oC. However, at 60 ^oC, all ion exchangeable binders exhibited more stable cycle performance than PVdF due to the ion exchange (Fig. 21).

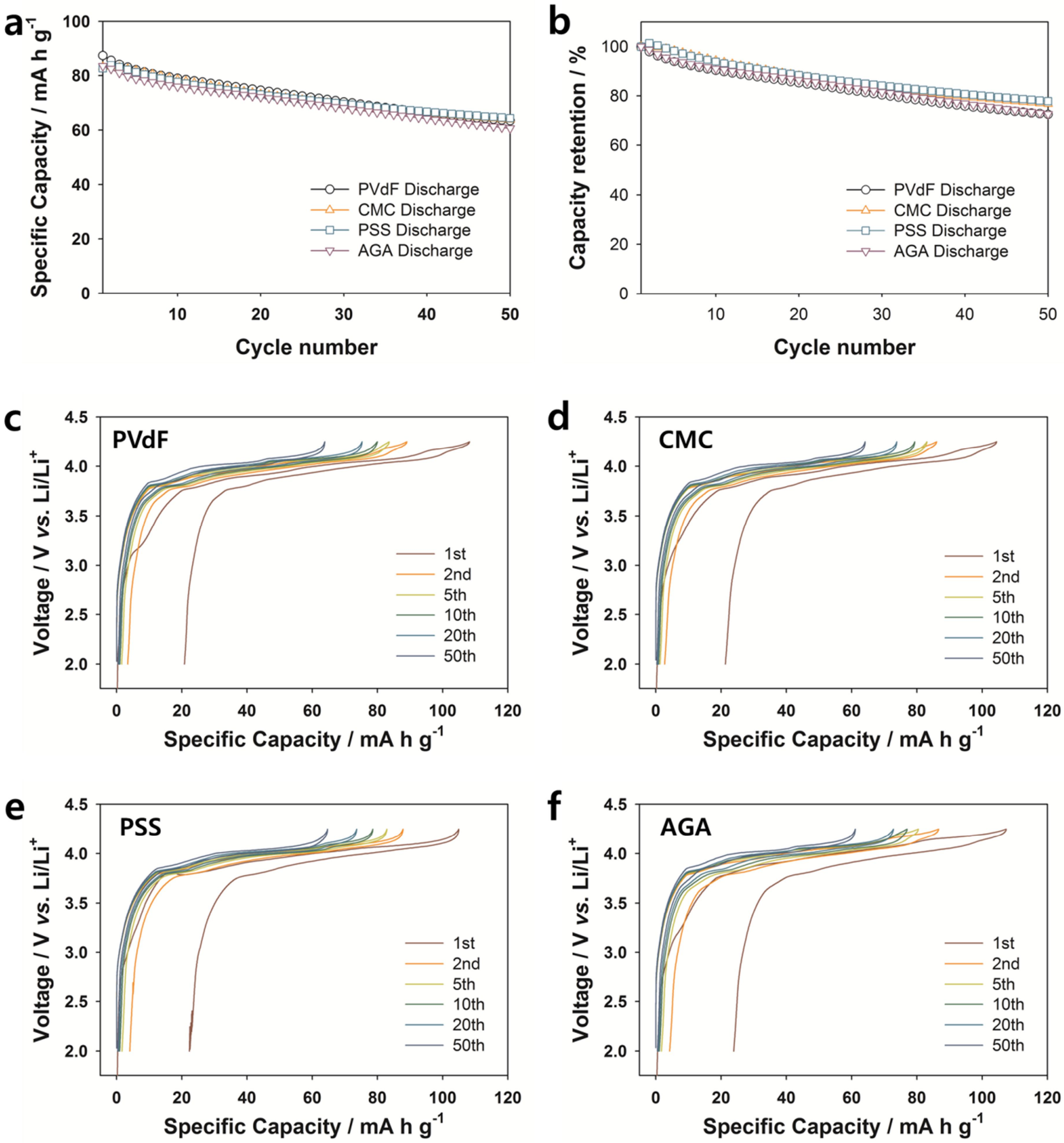

Figure 20. Electrochemical performances of $Li_{1.1}Mn_{1.86}Mg_{0.04}O_4$ (PVdF) / graphite (binder) full cell at 30 °C: a) cyclability, b) capacity retention, voltage profiles $Li_{1.1}Mn_{1.86}Mg_{0.04}O_4$ (PVdF) full cell with c) graphite (PVdF), d) graphite (CMC), e) graphite (PSS), and f) graphite (AGA).

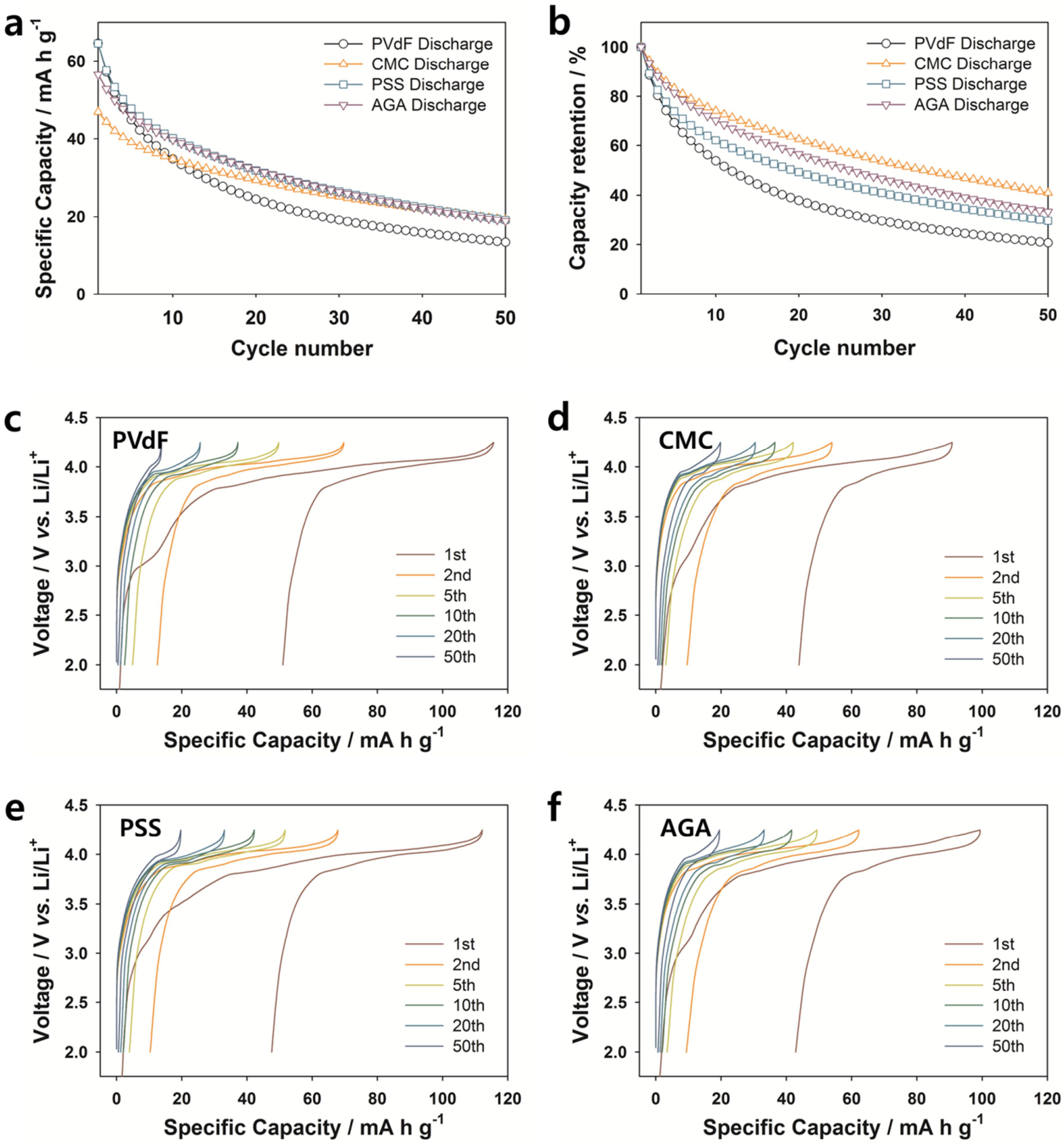

Figure 21. Electrochemical performances of $Li_{1.1}Mn_{1.86}Mg_{0.04}O_4$ (PVdF) / graphite (binder) full cell at 60 ^oC: a) cyclability, b) capacity retention, voltage profiles $Li_{1.1}Mn_{1.86}Mg_{0.04}O_4$ (PVdF) full cell with c) graphite (PVdF), d) graphite (CMC), e) graphite (PSS), and f) graphite (AGA).

The ion exchange between dissolved Mn^{2+} ions and Na^{+} ions of binders is supported by three designed experiments. First of all, the Na^{+} and Mn^{2+} concentrations in electrolytes were measured via inductively coupled plasma mass spectrometry (ICP-MS) before and after ion exchange occurred. Mn-dissolved electrolyte solution was prepared via storage of $Li_{1.1}Mn_{1.86}Mg_{0.04}O_4$ powders in $LiPF_6$-dissolved EC:DMC solution at 60 °C for 1 week, and then $Li_{1.1}Mn_{1.86}Mg_{0.04}O_4$ powders were removed through filtration. A considerable amount of manganese ions were dissolved in electrolyte at 60 °C, and Mn^{2+} concentration of the electrolyte solution was 0.14 mmol/kg. Powders of each binder was then added in the obtained manganese-dissolved electrolyte solution using a same weight ratio of binder/solution (300 mg/5 ml), and stored for 1 week. The binders were removed through filtration again, and the change of Na^{+} and Mn^{2+} concentrations of the resulting solutions were measured. As shown in Figure 22, Mn^{2+} concentration of the electrolyte solution slightly decreased into 0.98 mmol/kg after storage of the PVdF binder, but the other ion exchangeable binders showed that the negligible amount of Mn^{2+} was remained in the electrolytes and the concentration of Na^{+} was highly increased after storage of binders. This implies that Mn^{2+} is bound to functional group of binders due to ion exchange. Also, after storage of ion exchangeable binders, the Na^{+} concentration is observed much more than the expected value from ion exchange with Mn^{2+} in electrolytes, and this is attributed to the ion exchange between Li^{+} of $LiPF_6$ salts and Na^{+} of binders. Also, the ion exchange is further supported by that the IR spectra of the alginic acid binder is changed before and after storage in the manganese-dissolved solution (Fig. 23). The peak for symmetric carboxylate stretch was shifted from 1410 cm^{-1} to 1420 cm^{-1} after ion exchange. Finally, the change of XRD patterns of fully lithiated graphite electrodes (LiC_6) was observed before and after ion exchange due to the self-discharge. Half cells of graphite electrodes were first fully discharged when the redox potential reaches to 0V vs. Li/Li^{+}. Then, the cells were disassembled and the graphite electrodes were soaked in the manganese-dissolved electrolyte. After various soaking times from 0 to 60 min, the XRD patterns of the lithiated graphite electrodes were obtained. As shown in Figure 24, the lithiated graphite electrodes (LiC_6) prepared with the PVdF binder showed the formation of secondary phase of LiC_{12} after 10 min, and the mixture composed of LiC_{12} and LiC_{24} phases were observed after 60 min accompanying with disappearance of LiC_6 phase. This is attributed to that dissolved Mn^{2+} ions were reduced into Mn metal with the oxidation of the lithiated graphite. However, in the case of the lithiated graphite electrodes (LiC_6) with CMC binder, the negligible formation of LiC_{12} phase is observed even after 60 min, because most of dissolved Mn^{2+} ions were preferentially exchanged with Na^{+} ions of binders, resulting in inhibiting self-discharge.

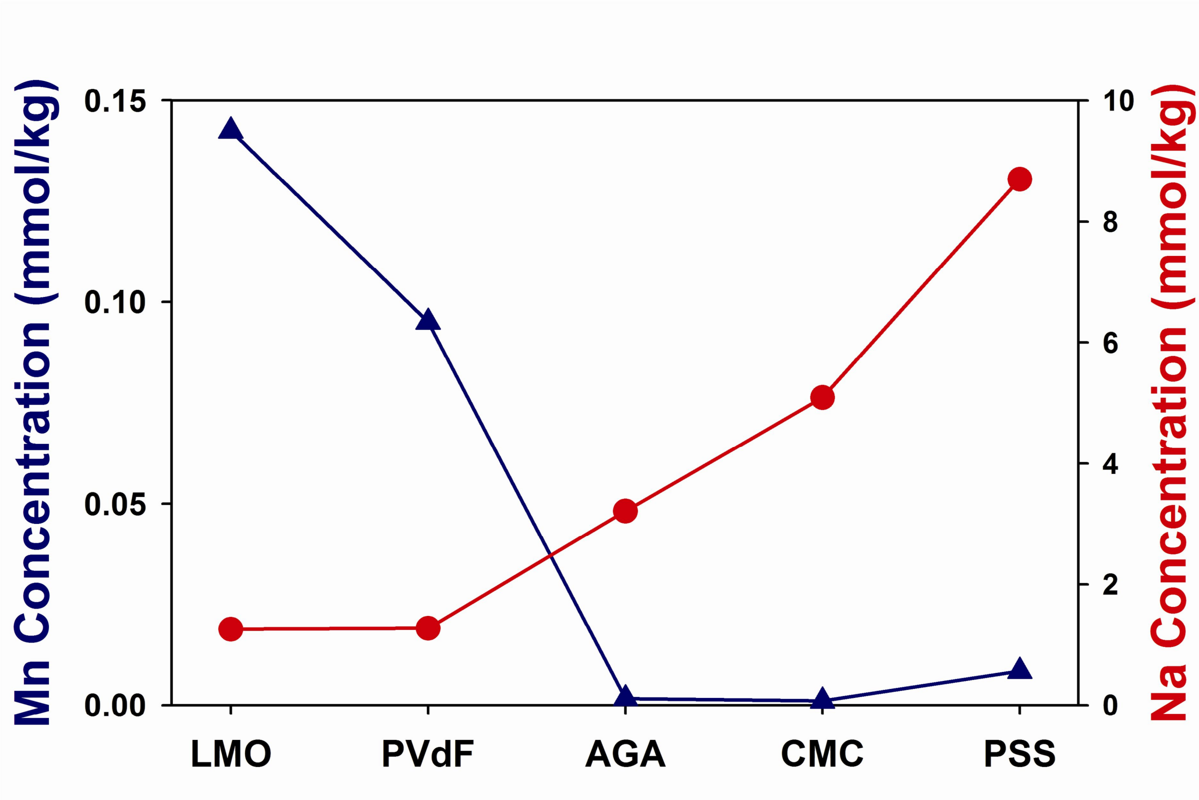

Figure 22. Mn and Na concentrations in an electrolyte before and after storage with binders.

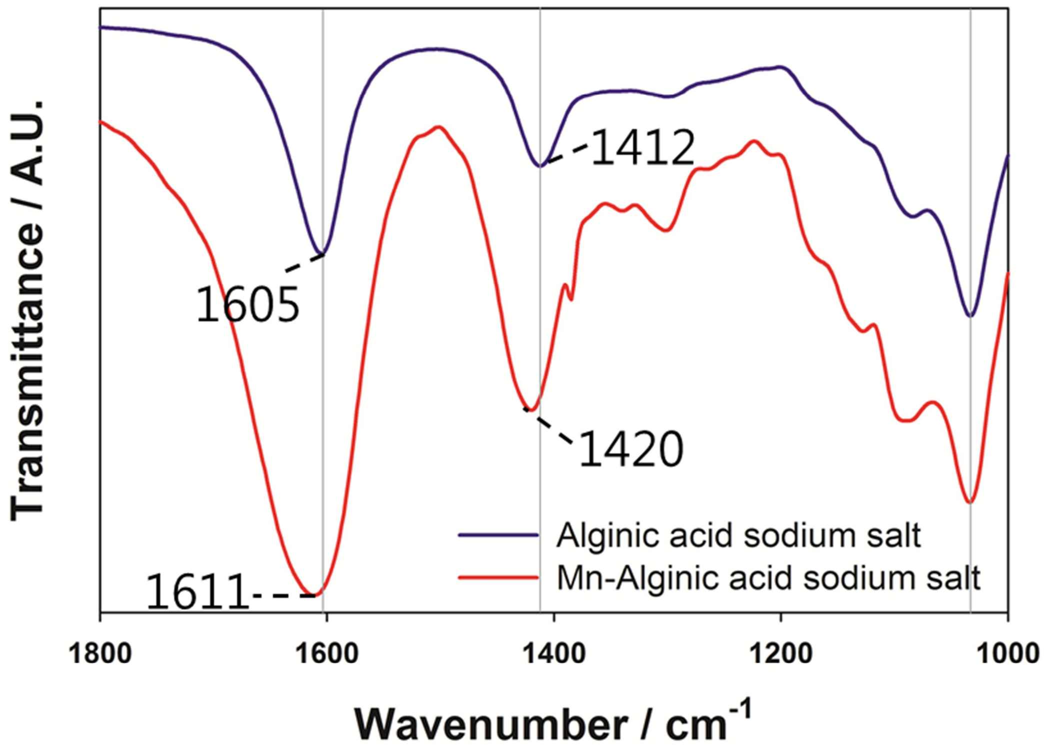

Figure 23. FT-IR spectra for alginic acid sodium salt before and after storage in the manganese-dissolved solution.

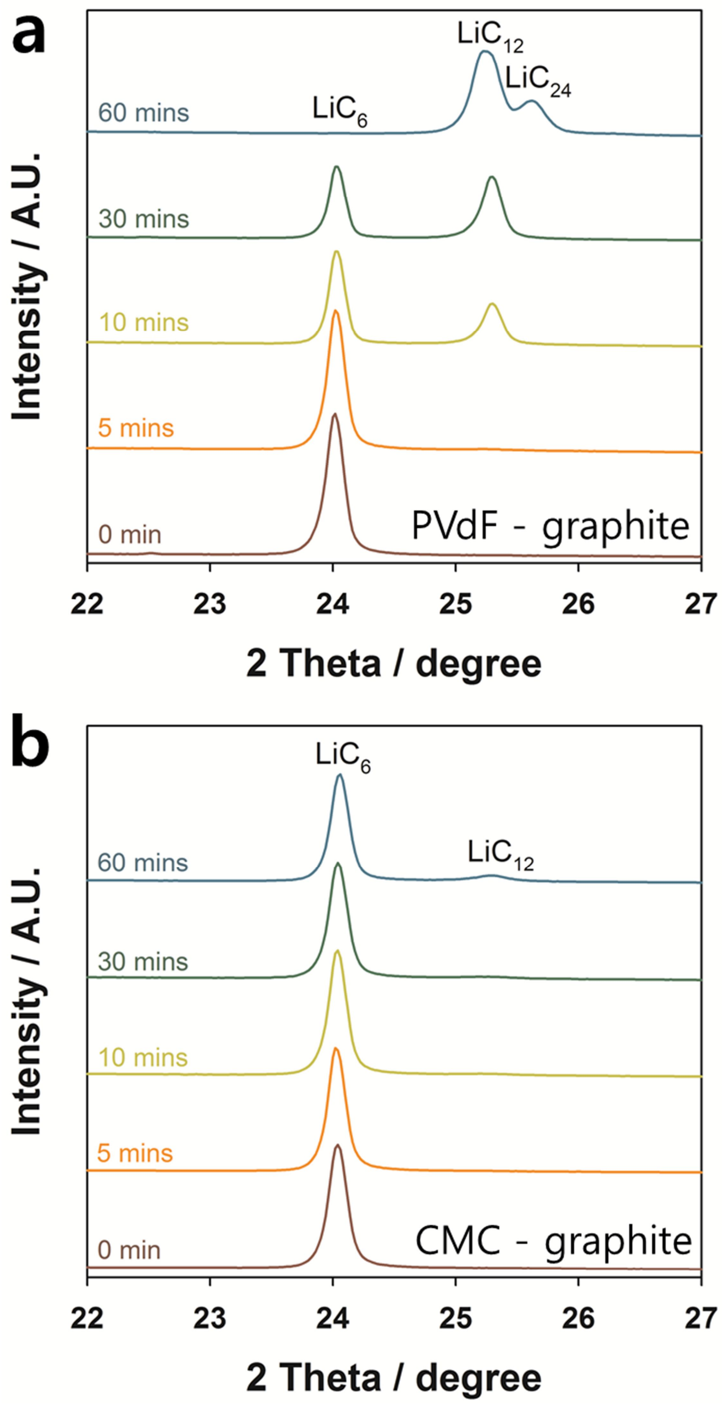

Figure 24. XRD patterns of lithiated graphite prepared with a) PVdF and b) CMC binder.

In addition, the ion exchangeable separator having a functional group of sodium carboxylate was synthesized to improve cycle performance of the $Li_{1.1}Mn_{1.86}Mg_{0.04}O_4$ electrode, as shown in the schematic diagram (Fig. 13). First, Al_2O_3 is homogenously coated on conventional polyethylene (PE) separators via atomic layer deposition (ALD) method. Because the typical growth rate for Al_2O_3 ALD is 1.1 - 1.2 Å per ALD cycle,[47-48] separator after 10 cycles ALD remain porous (Fig.25). Al_2O_3 is hydroxylized with treatment of H_2O_2. Then, 3-Aminopropyltriethoxysilane (APTES) was grafted on the surface of hydroxylized Al_2O_3. Carboxylic acid group of terephthalic acid is further reacted with amine group of grafted APTES by formation of amide group. Finally, carboxylic acid groups of the functionalized separator are changed into sodium carboxylate by treatment with NaOH. This synthesis is supported by IR spectra and XPS profile of surface-treated separators, as shown in Figure 26 and Figure 27, respectively. From IR spectra broad peaks at near 1000~1200 cm^{-1} are observed after treatment with APTES, and this indicates Si-O-Si stretching of APTES. After the reaction of terephthalic acid with APTES, the peaks at 1530 cm^{-1} and 1630 cm^{-1} are observable, indicating aromatic ring of teretphthalic acid and amide group, respectively. To clarify reaction of terephthalic acid, separator synthesized with terepahalic acid grafted iodine was used for XPS analysis. From XPS profile it is ascertained that terephthalic acid were grafted well onto the separator. Figure 28 shows the cycle performance of full cells at 60 ^{o}C and the corresponding voltage profiles. Full cells are comprised of $Li_{1.1}Mn_{1.86}Mg_{0.04}O_4$ spinel cathode with graphite anode, and electrodes are prepared with PVdF binders. It is notable that the ion exchangeable separator improved cycle performance at 60 ^{o}C, and this is attributed to the ion exchange between dissolved Mn^{2+} ions and Na^+ ions of the surface-treated separator with sodium terephtalate. This is supported by the decrease of Mn^{2+} concentration in the electrolyte from 0.082 mmol/L to 0.009 mmol/L after storage of the surface-treated separator in the manganese-dissolved electrolyte for 1 week.

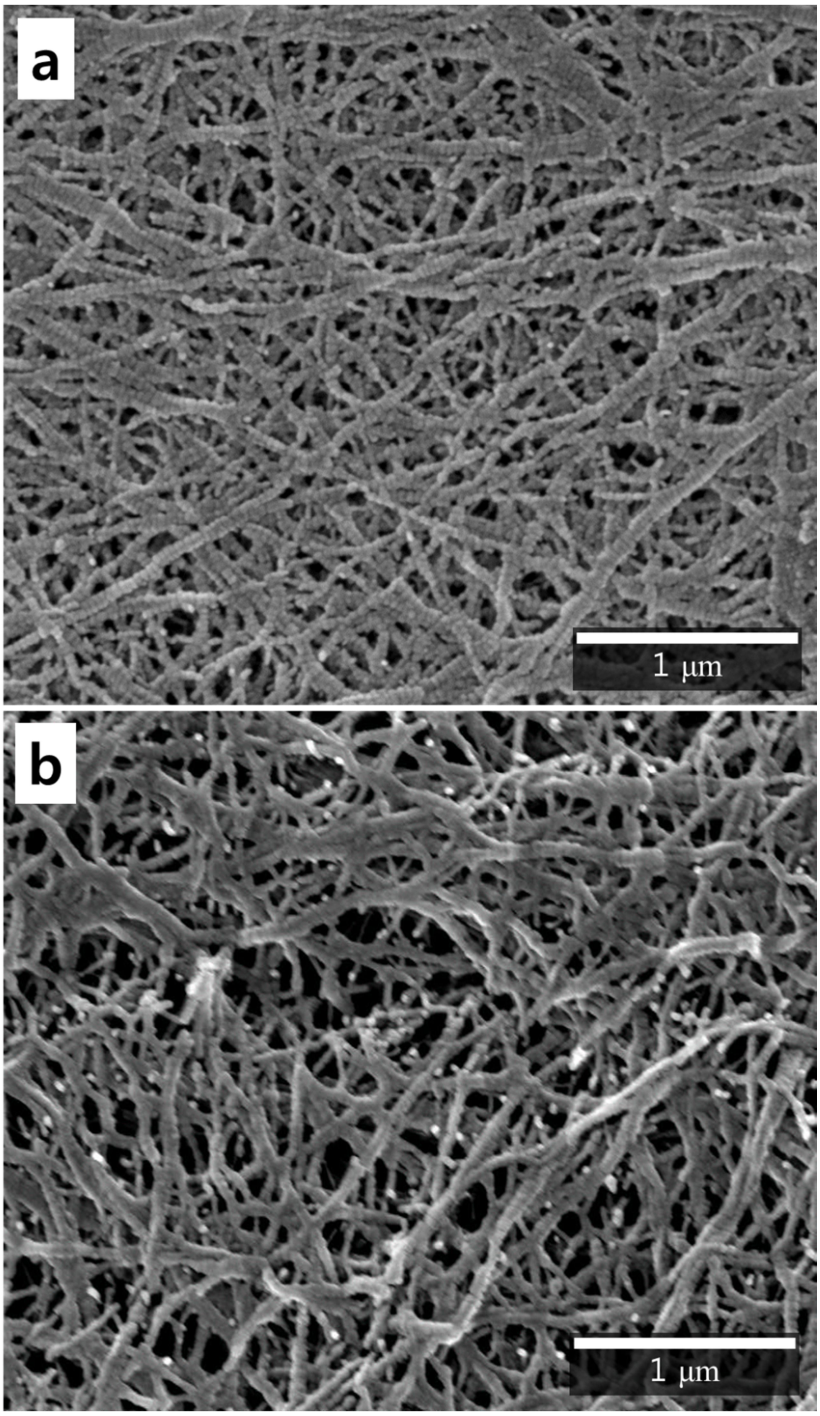

Figure 25. SEM images of a) PE bare separator and b) PE separator after 10 cycles ALD.

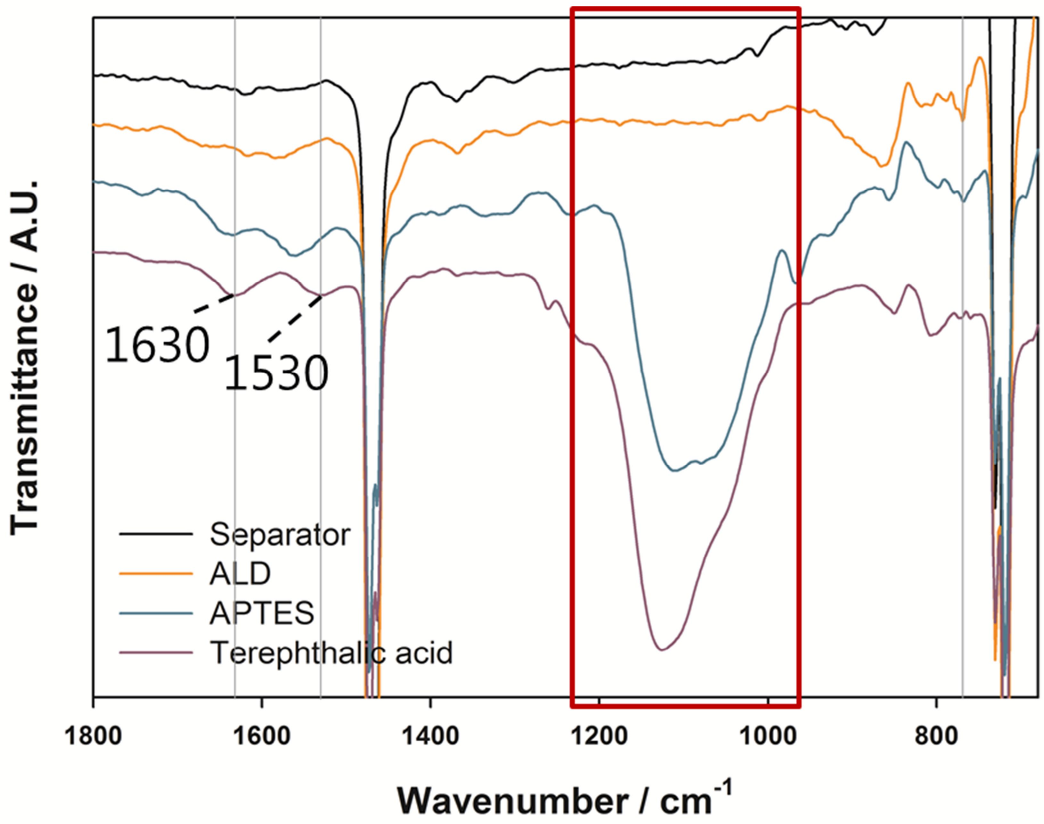

Figure 26. FT-IR spectra of separator according to priority of reaction.

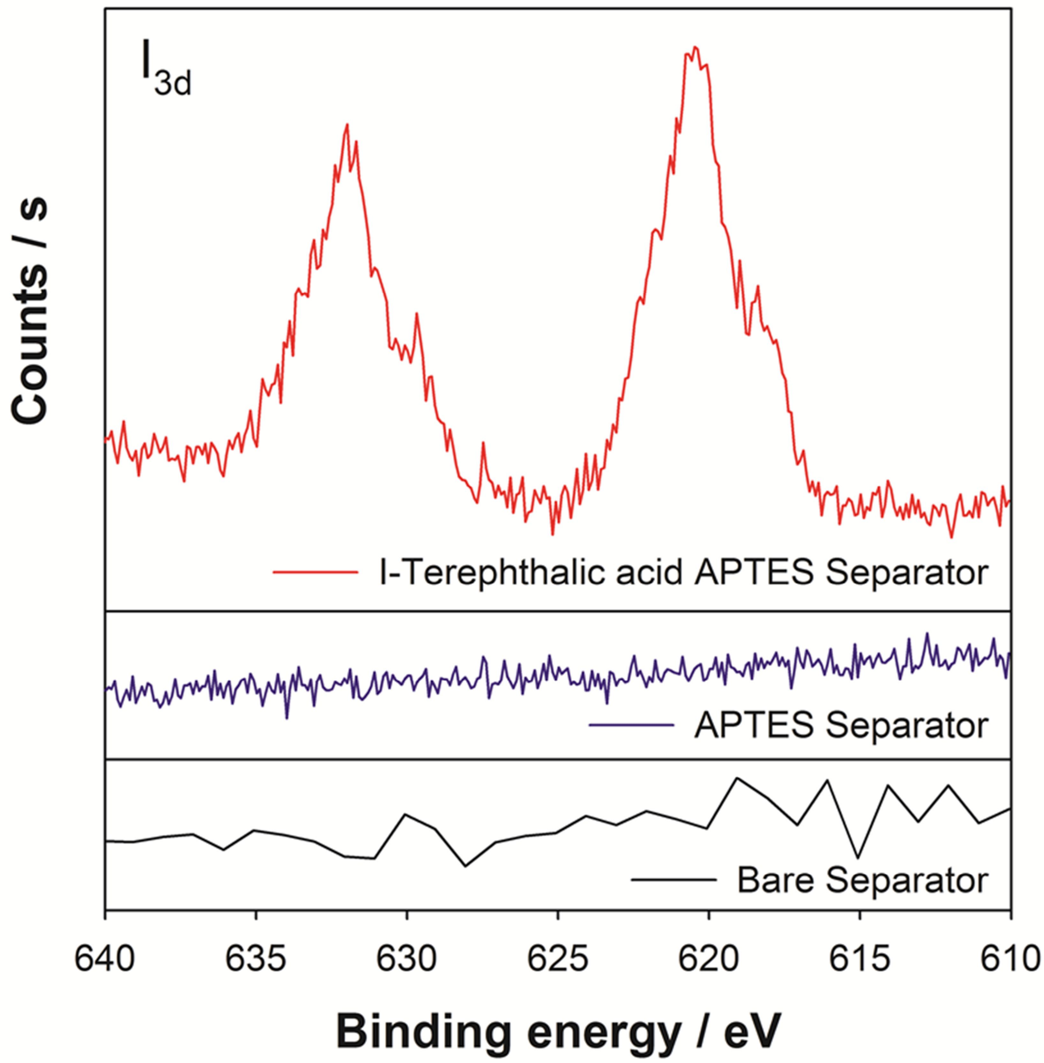

Figure 27. XPS profile of separator synthesized with terephthalic acid grafted with iodine.

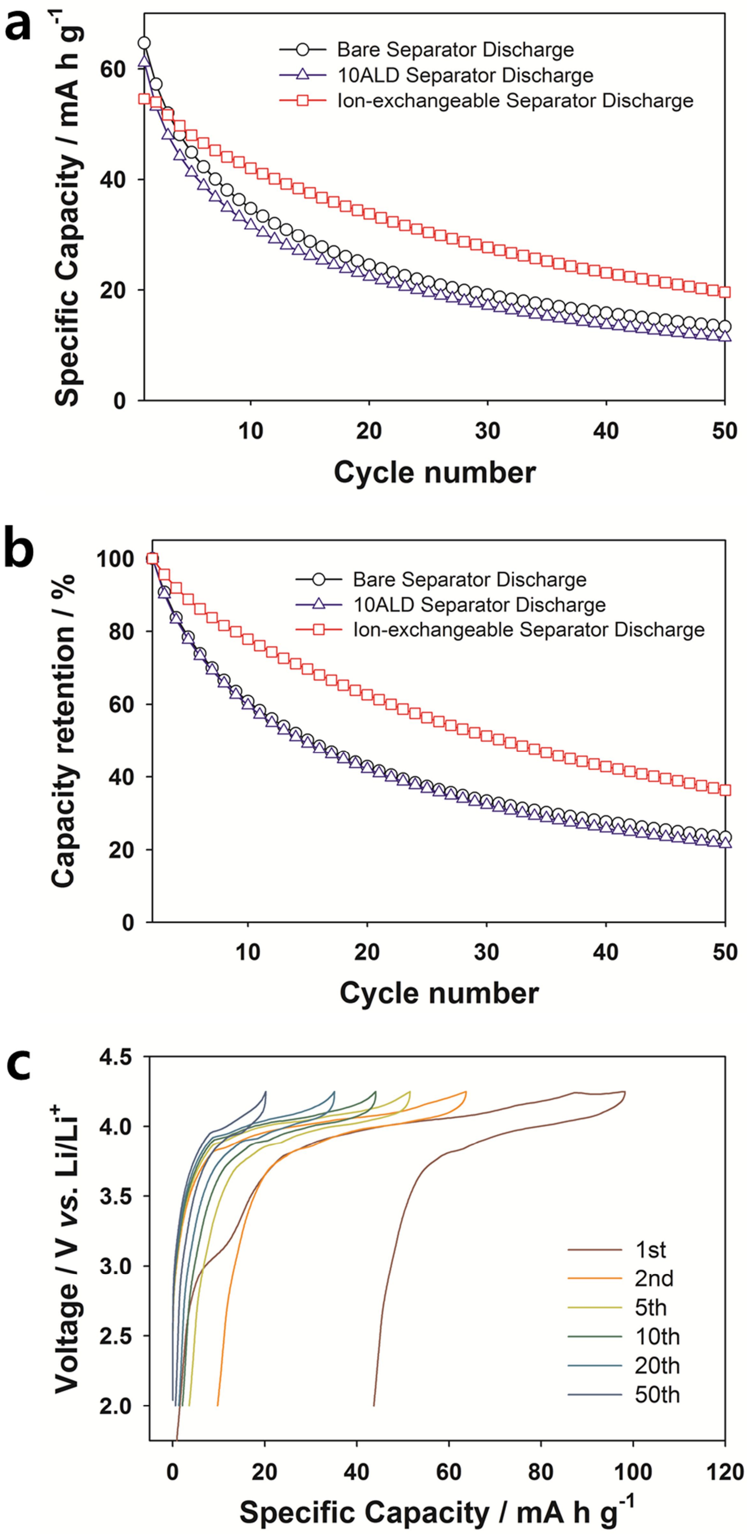

Figure 28. Electrochemical performances of $Li_{1.1}Mn_{1.86}Mg_{0.04}O_4$ (PVdF) / graphite (binder) full cell at 60 ^oC: a) cyclability, b) capacity retention, and c) voltage profiles of full cell with ion-exchangeable separator.

5. Conclusion

The ion-exchangeable binders and separator having functional groups of sodium carboxylate or sulfonate are, for the first time, suggested and examined for the improvement of high temperature cycle performance of $Li_{1.1}Mn_{1.86}Mg_{0.04}O_4$ spinel cathode materials. These functional groups of binders and separator cause the ion exchange between Na^+ ions of functional groups and dissolved Mn^{2+} ions of $LiMn_2O_4$ electrodes. This results in the trapping of dissolved Mn^{2+} ions to inhibit the reduction of Mn^{2+} on the surface of lithiated graphite anode. In this report, sodium carboxymethyl cellulose (CMC), poly(styrene sulfonate) (PSS) and alginate (AGA) were utilized as a function binder, and surface-treated separator with sodium terephthalate was synthesized for the ion exchangeable separator. Using these functional binders and separator, the cycle performance of $Li_{1.1}Mn_{1.86}Mg_{0.04}O_4$ spinel at 60 ^oC was highly improved due to ion exchange. The effect of ion exchange was supported by IR spectra of binders, ICP analysis of electrolytes and ex situ XRD patterns of lithiated graphite electrodes.

References

1. Megahed, S., Scrosati, B., ‘Lithium-ion rechargeable batteries’, *Journal of Power Sources*, **1994**, *51*, 79-10.

2. Nishi, Y., ‘Lithium ion secondary batteries; past 10 years and the future’, *Journal of Power Sources*, **2001**, *100*, 101-106.

3. Yoshio, M., Brodd, R. J., Kozawa, A. (Eds.), ‘Lithium-Ion Batteries: Science and Technologies’, *Springer*, **2009**.

4. Tarascon, J. -M., Armand, M., ‘Issues and challenges facing rechargeable lithium batteries’, *NATURE*, November **2001**, *414*, 15.

5. Bruce, P. G., Scrosati, B., Tarascon, J. –M., ‘Nanomaterials for Rechargeable Lithium Batteries’, *Angew. Chem. Int. Ed.*, **2008**, *47*, 2930-2946.

6. Song, H. -K., Lee, K. T., Kim, M. G., Nazr, L. F., Cho, J., ‘Recent Progress in Nanostructured Cathode Materials for Lithium Secondary Batteries’, *Adv. Funct. Mater.*, **2010**, *20*, 3818-3834.

7. Goodenough , J. B., Park, K. -S., ‘The Li-Ion Rechargeable Battery: A Perspective’, *J. Am. Chem. Soc.*, **2013**, *135*, 1167-1176.

8. Tarascon, J. M., Guyomard, D., ‘Li Metal-Free Rechargeable Batteries Based on $Li_{1+x}Mn_2O_4$ Cathodes ($0 \leq x \leq 1$) and Carbon Anodes’, *J. Electrochem. Soc.*, October **1991**, Vol. 138, No. 10.

9. Xia, Y., Yoshio, M., ‘An Investigation of Lithium Ion Insertion into Spinel Structure Li-Mn-O Compounds’, *J. Electrochem. Soc.*, March **1996**, Vol. 143, No.3.

10. Amine, K., Liu, J., Kang, S., Belharouak, I., Hyung, Y., Vissers, D., Henriksen, G., ‘Improved lithium manganese oxide spinel/graphite Li-ion cells for high-power applications’, *Journal of Power Sources*, **2004**, *129*, 14-19.

11. Kim, D. K., Muralidharan, P., Lee, H. -W., Ruffo, R., Yang, Y., Chan, C. K., Peng, H., Huggins, R. A., Cui, Y., ‘Spinel $LiMn_2O_4$ Nanorods as Lithium Ion Battery Cathodes’, *Nano Lett.*, **2008**, Vol. 8, No. 11.

12. Hosono, E., Kudo, T., Honma, I., Matsuda, H., Zhou, H., 'Synthesis of Single Crystalline Spinel $LiMn_2O_4$ Nanowires for a Lithium Ion Battery with High Power Density', *Nano Lett.*, **2009**, Vol. 9, No. 3.

13. Xia, Y., Takeshige, H., Noguchi, H., Yoshio, M., 'Studies on an Li-Mn-O spinel system (obtained by melt-impregnation) as a cathode for 4 V lithium batteries; Part 1. Synthesis and electrochemical behaviour of $Li_xMn_2O_4$', *Journal of Power Sources*, **1995**, *56*, 61-67.

14. Xia, Y., Yoshio, M., 'Studies on Li-Mn-O spinel system (obtained from melt-impregnation method) as a cathode for 4 V lithium batteries; Part IV. High and low temperature performance of $LiMn_2O_4$', *Journal of Power Sources*, **1997**, *66*, 129-133.

15. Xia, Y., Hideshima, Y., Kumada, N., Nagano, M., Yoshio, M., 'Studies on Li-Mn-O spinel system (obtained from melt-impregnation method) as a cathode for 4 V lithium batteries; Part V. Enhancement of the elevated temperature performance of Li/$LiMn_2O_4$ cells', *Journal of Power Sources*, **1998**, *24*, 24-28.

16. Inoue, T., Sano, M., 'An Investigation of Capacity Fading of Manganese Spinels Stored at Elevated Temperature', *J. Electrochem. Soc.*, November **1998**, Vol. 145, No. 11.

17. Gao, Y., Dahn, J. R., 'Correlation between the growth of the 3.3 V discharge plateau and capacity fading in $Li_{1+x}Mn_{2-x}O_4$ materials', *Solid State Ionics*, **1996**, *84*, 33-40.

18. Xia, Y., Zhou, Y., Yoshio, M., 'Capacity Fading on Cycling of 4 V Li/$LiMn_2O_4$ Cells', *J Electrochem. Soc.*, August **1997**, Vol. 144, No. 8.

19. Yang, L., Takahashi, M., Wang, B., 'A study on capacity fading of lithium-ion battery with manganese spinel positive electrode during cycling', *Electrochim. Acta*, **2006**, *51*, 3228-3234.

20. Ohzuku, T., Kitagawa, M., Hirai, T., 'Electrochemistry of Manganese Dioxide in Lithium Nonaqueous Cell; III. X-Ray Diffractional Study on the Reduction of Spinel-Related Manganese Dioxide', *J. Electrochem. Soc.*, March **1990**, Vol. 137, No. 3.

21. Gummow, R. J., Kock, A., Thackeray, M. M., 'Improved capacity retention in rechargeable 4 V lithium/lithium manganese oxide (spinel) cells', *Solid State Ionics*, **1994**, *69*, 59-67.

22. Sugiyama, J., Tamura, T., Yamauchi, H., 'Elastic/anelastic behaviour during the phase transition in spinel $LiMn_2O_4$', *J. Phys.: Condens. Matter*, **1995**, *7*, 9755-9764.

23. Hirayama, M., Ido, H., Kim, K. S., Cho, W., Tamura, K., Mizuki, J., and Kanno, R., 'Dynamic Structural Changes at $LiMn_2O_4$/Electrolyte Interface during Lithium Battery Reaction', *J. Am. Chem. Soc.*, **2010**, Vol. 132, No. 43.

24. Shao-Horn, Y., Hackney, S. A., Kahaian, A. J., Kepler, K. D., Skinner, E., Vaughey, J. T., Thackeray, M. M., 'Structural fatigue in spinel electrodes in $Li/Li_x[Mn_2]O_4$ cells', *Journal of Power Sources*, **1999**, *81-82*, 496-499.

25. Choi, N. -S., Yeon, J. -T., Lee, Y. -W., Han, J. -G., Lee, K. T., Kim, S. –S., 'Degradation of spinel lithium manganese oxides by low oxidation durability of $LiPF_6$-based electrolyte at 60 °C', *Solid State Ionics*, **2012**, *219*, 41-48.

26. Cho, I. H., Kim, S. -S., Shin, S. C., Choi, N. -S., 'Effect of SEI on Capacity Losses of Spinel Lithium Manganese Oxide/Graphite Batteries Stored at 60 °C', *Electrochem. Solid-State Lett.*, **2010**, *13* (11), A168-A172.

27. Park, S. B., Lee, S. M., Shin, H. C., Cho, W. I., Jang, H., 'An alternative method to improve the electrochemical performance of a lithium secondary battery with $LiMn_2O_4$', *Journal of Power Sources*, **2007**, *166*, 219-225.

28. Shi, S., Wang, D., Meng, S., Chen, L., Huang, X., 'First-principles studies of cation-doped spinel $LiMn_2O_4$ for lithium ion batteries', *PHYSICAL REVIEW*, **2003**, *B 67*, 115130.

29. Takahashi, M., Yoshida, T., Ichikawa, A., Kitoh, K., Katsukawa, H., Zhang, Q., Yoshio, M., 'Effect of oxygen deficiency reduction in Mg-doped Mn-spinel on its cell storage performance at high temperature', *Electrochimica Acta*, **2006**, *51*, 5508-5514.

30. Yang, S. T., Jia, J. H., Ding, L., Zhang, M. C., 'Studies of structure and cycleability of $LiMn_2O_4$ and $LiNd_{0.01}Mn_{1.99}O_4$ as cathode for Li-ion batteries', *Electrochim. Acta*, **2003**, *48*, 569-573.

31. Capsonia, D., Binia, M., Chiodellia, G., Massarottia, V., Mustarellia, P., Linati, L., Mozzatic, M. C., Azzoni, C. B., 'Jahn-Teller transition in Al^{3+} doped $LiMn_2O_4$ spinel', *Solid State Communications*, **2003**, *126*, 169-174.

32. Lu, C. -H., Wang, H. -C., 'Effects of cobalt-ion doping on the electrochemical properties of spinel lithium manganese oxide prepared via a reverse-micelle route', *Journal of the European Ceramic Society*, **2003**, *23*, 865-871.

33. Nieto, S., Majumder, S. B., Katiyar, R. S., 'Improvement of the cycleability of nano-crystalline lithium manganate cathodes by cation co-doping', *Journal of Power Sources*, **2004**, *136*, 88-98.

34. Liu, X., Wang, J., Zhang, J., Yang, S., 'Fabrication and characterization of Zr and Co co-doped $LiMn_2O_4$ nanowires using sol-gel-AAO template process', *J Mater Sci: Mater Electron*, **2006**, *17*, 865-870.

35. Suryakala, K., Kalaignan, G. P., Vasudevan, T., 'Synthesis and characterization of Cr-doped $LiMn_{2-x}Cr_xO_4$ (x = 0.1-0.4) cathode for Li-ion battery', *Materials Chemistry and Physics*, **2007**, *104*, 479-482.

36. Wu, H. M., Tu, J. P., Chen, X. T., Li, Y., Zhao, X. B., Cao, G. S., 'Effects of Ni-ion doping on electrochemical characteristics of spinel $LiMn_2O_4$ powders prepared by a spray-drying method', *J. Solid State Electrochem.*, **2007**, *11*, 173-176.

37. Singhal, R., Das, S. R., Tomar, M. S., Ovideo, O., Nieto, S., Melgarejo, R. E., Katiyar, R. S., 'Synthesis and characterization of Nd doped $LiMn_2O_4$ cathode for Li-ion rechargeable batteries', *Journal of Power Sources*, **2007**, *164*, 857-861.

38. Kannan, A. M., Manthiram, A., 'Surface/Chemically Modified $LiMn_2O_4$ Cathodes for Lithium-Ion Batteries', *Electrochem. Solid-State Lett.*, **2002**, *5* (7), A167-A169.

39. Zheng, Z., Tang, Z., Zhang, Z., Shen, W., Lin, Y., 'Surface modification of $Li_{1.03}Mn_{1.97}O_4$ spinels for improved capacity retention', *Solid State Ionics*, **2002**, *148*, 317-321.

40. Gnanaraj, J. S., Pol, V. G., Gedanken, A., Aurbach, D., 'Improving the high-temperature performance of $LiMn_2O_4$ spinel electrodes by coating the active mass with MgO via a sonochemical method', *Electrochem. Comm.*, **2003**, *5*, 940-945.

41. Lim, S. H., Cho, J., 'PVP-Assisted ZrO_2 coating on $LiMn_2O_4$ spinel cathode nanoparticles prepared by MnO_2 nanowire templates', *Electrochem. Comm.*, **2008**, *10*, 1478-1481.

42. Arumugam, D., Kalaignan, G. P., 'Synthesis and electrochemical characterizations of Nano-SiO_2-coated $LiMn_2O_4$ cathode materials for rechargeable lithium batteries', *Journal of Electroanalytical Chemistry*, **2008**, *624*, 197-204.

43. Lee, S., Cho, Y., Song, H. -K., Lee, K. T., Cho, J., 'Carbon-Coated Single-Crystal $LiMn_2O_4$ Nanoparticle Clusters as Cathode Material for High-Energy and High-Power Lithium-Ion Batteries', *Angew. Chem. Int. Ed.*, **2012**, *51*, 8748 -8752.

44. Tsunekawa, H., Tanimoto, S., Marubayashi, R., Fujita, M., Kifune, K., Sano, M., 'Capacity Fading of Graphite Electrodes Due to the Deposition of Manganese Ions on Them in Li-Ion Batteries', *J. Electrochem. Soc.*, **2002**, *149* (10) A1326-A1331.

45. Liu, Y., Li, X., Guo, H., Wang, Z., Hu, Q., Peng, W., Yang, Y., 'Electrochemical performance and capacity fading reason of $LiMn_2O_4$/graphite batteries stored at room temperature', *Journal of Power Sources*, **2009**, *189*, 721-725.

46. Alchin, D., Wansbrough, H., 'XIII-Water-D-Ion Exchange Resins'.

47. Jung, Y. S., Cavanagh, A. S., Dillon, A. C., Groner, M. D., George, S. M., Lee, S. –H., 'Enhanced Stability of $LiCoO_2$ Cathodes in Lithium-Ion Batteries Using Surface Modification by Atomic Layer Deposition', *J. Electrochem. Soc.*, **2010**, *157*, A75-A81.

48. Jung, Y. S., Cavanagh, A. S., Gedvilas, L., Widjonarko, N. E., Scott, I. D., Lee, S. -H., Kim, G. -H., George, S. M., Dillon, A. C., 'Improved Functionality of Lithium-Ion Batteries Enabled by Atomic Layer Deposition on the Porous Microstructure of Polymer Separators and Coating Electrodes', *Adv. Energy Mater.*, **2012**, *2*, 1022-1027.